communications medicine

A Nature Portfolio journal

Article

https://doi.org/10.1038/s43856-025-01170-5

Integrating individualized connectome with amyloid pathology improves predictive modeling of future cognitive decline

Hengda He[1] ✉, Qolamreza R. Razlighi[2], Yunglin Gazes[3], Christian Habeck[1,4,5], Yaakov Stern[1,4,5] ✉ & for the Alzheimer's Disease Neuroimaging Initiative*

Abstract

Background The deposition of amyloid-β (Aβ) in the human brain is a hallmark of Alzheimer's disease and is associated with cognitive decline. Aβ pathology is traditionally assessed at the whole-brain level across neocortical regions using positron emission tomography (PET). However, these measures often show weak associations with future cognitive impairment. A more sensitive pathology metric is needed to quantify early Aβ burden and better predict cognitive decline. Here, we aim to develop a network-based metric of Aβ burden to improve early prediction of cognitive decline in aging populations.

Methods We integrated subject-specific brain connectome information with Aβ-PET measures to construct a network-based metric of Aβ burden. Cross-validated predictive modeling was used to evaluate the performance of this metric in predicting longitudinal cognitive decline. Furthermore, we identified a neuropathological signature pattern linked to future cognitive decline, and we validated this pattern in an independent cohort.

Results Our results demonstrate that incorporating individualized structural connectome, but not functional connectome, information into Aβ measures enhances predictive performance for prospective cognitive decline. The identified neuropathological signature pattern is reproducible across cohorts.

Conclusion These findings advance our understanding of the spatial patterns of Aβ pathology and its relationship to brain networks, highlighting the potential of connectome-informed network-based metrics for Aβ-PET imaging in identifying individuals at higher risk of cognitive decline.

Plain language summary

Amyloid-β peptide is a molecule that is known to accumulate in the brains of people with Alzheimer's disease. This accumulation starts to occur many years before the symptoms of Alzheimer's disease, such as memory problems. Current methods to image the brain for amyloid-β peptide usually measure the overall level across the whole brain. In this study, we developed a more sensitive and personalized measure of amyloid-β by also considering how the different parts of a person's brain are connected. We found that this approach improves the ability to predict future changes in cognition compared to the standard method. Our method might enable earlier identification of people at risk of developing Alzheimer's disease, which could improve monitoring and treatment.

Amyloid-β (Aβ) pathology is recognized as one of the earliest initiating events in Alzheimer's disease (AD) progression. As proposed by the Amyloid-β Cascade Hypothesis[1,2], abnormal accumulation of Aβ in the brain has been linked to a cascade of pathological events, including tau tangle formation and spread[3,4], inflammation[5], gray matter atrophy[6], neuronal dysfunction and network disruption[7,8], and ultimately cognitive and functional impairment[9]. Aβ deposition is commonly observed in the brain in older adults who do not show significant cognitive impairment[10]. However, individuals with elevated Aβ pathology are at increased risk of developing dementia in the future[11], and are considered to be in the preclinical phase of AD[12]. In this study, we developed network-based amyloid-β pathology (NAP) measures that incorporate subject-specific connectome

[1]Cognitive Neuroscience Division, Department of Neurology, Vagelos College of Physicians and Surgeons, Columbia University, New York, NY, USA. [2]Quantitative Neuroimaging Laboratory, Brain Health Imaging Institute, Department of Radiology, Weill Cornell Medicine, New York, NY, USA. [3]Center for Biomedical Imaging & Neuromodulation, Nathan S. Kline Institute for Psychiatric Research, Orangeburg, NY, USA. [4]Taub Institute for Research in Alzheimer's Disease and the Aging Brain, Columbia University, New York, NY, USA. [5]Gertrude H. Sergievsky Center, Columbia University, New York, NY, USA. [49]Deceased: J.Q. Trojanowski. *A list of authors and their affiliations appears at the end of the paper. ✉e-mail: hh2699@cumc.columbia.edu; ys11@cumc.columbia.edu

information. We then examined how these neuropathology measures, assessed at baseline, are associated with cognitive changes over the subsequent years.

The literature presents heterogeneous findings regarding the relationship between Aβ and cognition. The most consistent associations have been observed in episodic memory[13–17]. However, the reported relationships between Aβ and cognition are often weak[15,18], and the results for non-memory cognitive domains are inconsistent. Some studies that assessed global cognition, combining measures across multiple cognitive domains, yielded slightly larger effect sizes, but such effects remain moderate[15].

In clinical settings, Aβ deposition is quantified dichotomously, classified as positive when above the cut-off threshold and negative when below it, and is measured globally across the entire cerebral cortex. However, the organization of brain network systems has been proposed as an important influencing factor in the relationship between neuropathology and clinical symptoms[19–21]. Therefore, effective metrics of early Aβ pathology that consider its spatial location and spread are needed, and may potentially facilitate earlier recognition and intervention[22].

Aβ deposition is spatially heterogeneous, especially in the preclinical phase of AD. Thus, some studies suggested that regional and continuous measures of Aβ deposition provide additional value in the early identification of participants at risk of transitioning from preclinical to clinical AD[14,23,24]. Early deposition has been shown to concentrate in the default mode network and other highly connected regions[7,25]. By exploring the spatial pattern and regional-temporal evolution of Aβ deposition, studies have suggested diverse pathological staging patterns[26–28]. Moreover, recent evidence indicates that early Aβ deposition patterns vary across individuals[24,29]. These spatially heterogeneous patterns may reflect the accumulation of neuropathology in distinct sets of brain networks, depending on the individualized connectome, and different networks may potentially be associated with distinct clinical symptoms. These findings highlight the need for integrating connectome and network information in Aβ-cognition studies.

In this study, we characterized the potential role of the brain network connectome on the Aβ-cognition relationship by employing network-based neuropathological measures of Aβ. We reasoned that these measures would provide a more comprehensive metric to capture the complex relationship between neuropathology and cognitive function. We developed NAP measures by incorporating connectome information that considers both initial regional Aβ burden and its deposition within individualized connectomes. Two types of connectomes were used independently: structural connectivity derived from diffusion magnetic resonance imaging (MRI) and functional connectivity derived from resting-state functional MRI. We then examined how these patterns, measured at baseline, are associated with cognitive changes over subsequent years. To improve the generalizability of our findings, we employed a cross-validated machine learning predictive model. Connectome-based predictive modeling (CPM)[30–32] has been widely used to study brain-behavior relationships, which leverages brain connectivity patterns to predict individual differences in behavior and cognition. Here, we adapted the CPM framework to evaluate the performance of the NAP measure in predicting subsequent longitudinal cognitive decline, and compare it to the predictive performance of the regional amyloid-β standardized uptake value ratio (SUVR) value using the positron emission tomography (PET) imaging of Aβ pathology. We hypothesized that integrating connectome information would improve the prediction of cognitive decline. We derived a neuropathological signature of cognitive decline, which provides insights into the regional-specific and network-level contributions of Aβ neuropathology to cognitive deterioration. We then sought external validation in the second cohort to confirm the neuropathological signature's association with future cognitive decline and demonstrate its generalizability. These results advance our understanding of Aβ pathology within brain network systems and offer a framework for future studies on Aβ deposition and cognition that incorporate personalized connectome profiles and brain network analyses. The proposed NAP measures could potentially better reflect the individual risk of future cognitive decline.

Methods

Participants and study design in the CogRes/RANN study

Participants were recruited through our ongoing cognitive reserve and reference ability neural network (CogRes/RANN) longitudinal study[33]. All participants were cognitively normal at baseline. They were screened for dementia and mild cognitive impairment (MCI) using the Dementia Rating Scale (DRS)[34]. A minimum score of 130 was required for the DRS assessment. Here, we included eighty-five cognitively normal older adults (Demographic information is in Table 1). All participants were recruited using a random market mailing approach and were screened for basic inclusion criteria (i.e., right-handed, native English-speaking, no severe medical or psychiatric conditions, no head injuries, no hearing or vision impairments, and no other issues that could interfere with MRI acquisition or cognition). Data were collected at Columbia University Irving Medical Center. The first participant was enrolled in 2011, and data collection is still ongoing. The experimental design of our study and the recruitment process were approved by the Institutional Review Board of the College of Physicians and Surgeons of Columbia University. All participants have provided informed consent to participate in the study, and written consent was obtained from the participants. All participants were scheduled for 5- and 10-year follow-ups. Multiple types of contact information were collected at baseline, and phone calls, emails, and regular mail were used to reach participants for follow-up. In this study, we included subjects who had: (1) participated in baseline MRI acquisitions and Aβ PET, (2) demographic information available at baseline, and (3) finished neuropsychological testing at both baseline and follow-up sessions. Data were available for eighty-five subjects, with a baseline age ranged from 56 to 71 (65.56 ± 3.35, mean ± SD) years, 42 females and 43 males, and education ranged from 12 to 20 (16.12 ± 2.22, mean ± SD) years. To perform cross-validated predictive model analyses with NAP, eight additional participants were excluded due to: (1) three subjects with functional connectivity results not passing quality control (QC); (2) five subjects with no baseline diffusion MRI data, leaving seventy-seven subjects.

Participants and study design in the ADNI study

Data used in the preparation of this article were obtained from the Alzheimer's Disease Neuroimaging Initiative (ADNI) database (adni.loni.usc.edu). The ADNI was launched in 2003 as a public-private partnership, led by Principal Investigator Michael W. Weiner, MD. The primary goal of ADNI has been to test whether serial MRI, PET, other biological markers, and clinical and neuropsychological assessment can be

Table 1 | Demographic information for the cognitive reserve and reference ability neural network (CogRes/RANN) longitudinal study and the Alzheimer's Disease Neuroimaging Initiative (ADNI) study datasets

Dataset	Number of participants	Baseline age (SD)	Sex	Education (SD), years	Time (SD) from baseline to follow-up neuropsychological assessments, years
CogRes/RANN	85	65.56 (3.35)	42(F)/43(M)	16.12 (2.22)	4.51 (0.68)
ADNI	72	73.69 (7.35)	46(F)/26(M)	16.83 (2.39)	ADNI-Mem and ADNI-GCog: 3.40 (1.18) dMemory: 3.34 (1.17)

The ADNI study dataset was used as an external dataset for generalizability validation.

combined to measure the progression of MCI and early AD. In this study, data from the ADNI phase 3 (ADNI-3) database were used as an external validation dataset. The ADNI study received approval from the Institutional Review Boards of all participating institutions, and informed written consent was obtained from all participants at each site for participating in the ADNI repository. In this study, we included a sample of 159 cognitively normal older adults from a previous study[35]. In ADNI, cognitively normal subjects were identified as non-depressed, non-MCI, non-demented, with Mini-Mental State Examination (MMSE) scores of 24–30 and clinical dementia rating scores close to zero. We excluded 12 participants due to progression to MCI in the follow-up, 44 participants with no diffusion data acquisition or missing information in diffusion data, 5 participants who failed with structural connectivity QC, 7 participants who failed with PET Aβ analysis, 18 participants without follow-up cognition available, and 1 participant without baseline education available. Totally, the external validation dataset consisted of 72 participants, with baseline age ranged from 56.0 to 91.4 (73.69 ± 7.35, mean ± SD) years, 46 females and 26 males, and education ranged from 12 to 20 (16.83 ± 2.39, mean ± SD) years. When testing the Aβ-cognition relationship with the ADNI memory score and the ADNI global cognition score, one additional participant was excluded due to the follow-up ADNI memory score not being available.

Cognitive behavioral measures in the CogRes/RANN study

A standardized battery of neuropsychological assessments was administered to assess four domains of cognition: (1) episodic memory (Selective Reminding Task immediate recall, delayed recall, and delayed recognition[36]); (2) vocabulary (Wechsler Adult Intelligence Scale (WAIS-III) Vocabulary[37], Wechsler Test of Adult Reading[38], and American National Adult Reading Test[37]); (3) processing speed (WAIS-III Digit Symbol[37], Stroop Color Word Test[39], and Trail-Making Test versions A[40]), and (4) fluid reasoning (WAIS-III Matrix Reasoning[37], WAIS-III Block Design[37], and Trail-Making Test versions B[40]). Based on the factor structure of these tests, cognitive composite scores for each cognitive domain were generated. To normalize the composite measures, *z*-scores were calculated within each domain by subtracting the baseline full sample mean from each score and then dividing by the baseline full sample standard deviation. The average domain *z*-score for processing speed was reversed in sign to ensure that higher values represented better cognitive performance. An average of the four *z*-scores of all four cognitive domains was calculated to yield a global cognition score. The baseline and follow-up neuropsychological assessments duration was 3–7 (4.51 ± 0.68, mean ± SD) years.

Cognitive behavioral measures in the ADNI study

Three ADNI cognition scores were assessed: (1) ADNI-Mem; (2) ADNI-GCog (summarized score of memory, executive functioning, and language); (3) delayed recall tests of memory (dMemory). ADNI-Mem was assessed with modern psychometric approaches[41], where Rey Auditory Verbal Learning Test (RAVLT, 2 versions), AD Assessment Schedule – Cognition (ADAS-Cog, 3 versions)[42], MMSE, and Logical Memory data were analyzed, and a composite memory score was computed. ADNI executive functioning score (ADNI-EF) was derived from confirmatory factor analysis, and the final model included Category Fluency—animals, Category Fluency—vegetables, Trails A and B, Digit span backward, WAIS-R Digit Symbol Substitution, and 5 Clock Drawing items (circle, symbol, numbers, hands, time). More details were described in ref. 43. ADNI language score (ADNI-Lan) was derived from MMSE (object naming, sentence repetition, sentence reading and writing, and following a three-step command), ADAS-Cog (following commands, object naming, and ideational praxis)[42], ADNI administered Montreal Cognitive Assessment (phonemic fluency and sentence repetition)[44]. More details are described in ref. 45. The three ADNI composite scores were averaged to compute an assessment of global cognition (ADNI-GCog). To further assess episodic memory, we additionally derived a dMemory score using delayed recall tests. Specifically, logical memory delayed total recall from the neuropsychological battery was converted to *z*-scores based on the baseline full sample mean and standard deviation from all cognitively normal older adults in ADNI-3. The same process was performed for the delayed word recall (item 4 of ADAS-Cog) to derive the *z*-scores. These two scores were averaged to obtain the dMemory score for assessing episodic memory. Follow-up cognition was chosen as the latest neuropsychological testing when multiple follow-up sessions were available. The baseline and follow-up neuropsychological assessments duration is 1 to 5.5 (3.40 ± 1.18, mean ± SD) years for ADNI-Mem and ADNI-GCog, and 1 to 5.5 (3.34 ± 1.17, mean ± SD) years for dMemory.

Data acquisition and preprocessing in the CogRes/RANN study

MR images were acquired using a 3 Tesla Philips Achieva Magnet scanner. An anatomical T1-weighted structural image was acquired using magnetization-prepared rapid gradient echo (MPRAGE) (TR/TE = 6.6/3.0 ms; flip angle = 8°; field of view (FOV) = 256 × 256 mm; matrix size = 256 × 256 voxels; voxel size = 1 × 1 × 1 mm; 165 axial slices). A neuroradiologist reviewed each participant's MRI scan and confirmed the absence of clinically significant findings in all participants. Resting-state fMRI scans were collected with a T2*-weighted echo-planar imaging (EPI) sequence (TR/TE = 2000/20 ms; flip angle = 72°; FOV = 224 × 224 mm; in-plane resolution = 112 × 112 voxels; slice thickness = 3 mm; 37 axial slices; either 150 or 285 volumes). Three dummy EPI volumes acquired at the beginning of each fMRI acquisition run were excluded before data preprocessing. Diffusion MR images were acquired with spin-echo echo-planar diffusion-weighted sequences. Participants' data were acquired with a single shell sequence (TR/TE = 7647/69 ms, matrix size = 224 × 224 mm, voxel size = 2 × 2 × 2 mm, 75 axial slices, $b = 800$ s/mm^2 with 56 gradient directions, and 1 volume with $b = 0$ s/mm^2). Two runs of diffusion MR were performed for each subject, and data were merged before preprocessing.

Structural T1-weighted MR images were processed using the FreeSurfer pipeline v5.1[46], which included segmentation of brain tissue, reconstruction of the cerebral cortex surface, and computation of cortical thickness. Hemispherical mean cortical thickness was computed as the average cortical thickness measures across 34 regions from the FreeSurfer Desikan-Killiany atlas[47] for each hemisphere. Brain parcellation was performed based on the Local-Global Schaefer cortical parcellation atlas[48] and FreeSurfer subcortical segmentation[49]. Specifically, 200 cortical regions of interest (ROIs) were defined using the Schaefer atlas. The Schaefer atlas was aligned to each subject's cortical surface through surface-based registration with FreeSurfer. Subsequently, the ROI surface areas were projected into volumetric space, resulting in the parcellation of the cerebral cortex into 200 ROIs. The Schaefer atlas grouped these 200 ROIs into 34 brain networks. Additionally, 14 subcortical ROIs were included from the FreeSurfer automatic segmentation[49] (regions included bilateral thalamus, caudate, putamen, ventral striatum, globus pallidus, amygdala, and hippocampus). Totally, 214 ROIs were used with 200 cortical regions from the Schaefer atlas and 14 subcortical regions from FreeSurfer segmentation. Tissue segmentation and spatial registration were manually reviewed for quality control purposes[50].

At baseline, participants underwent Aβ PET imaging with [^{18}F]Florbetaben (donated by Piramal Pharma, Inc.) in a Siemens Biograph64 mCT/PET scanner (dynamic, 3D acquisition mode, 4 × 5-min frames over 20 min). Brain PET image acquisition started 50 min after the bolus injection of 18F-florbetaben (10 mCi dose). An accompanying structural CT scan (in-plane resolution = 0.58 × 0.58 mm; slice thickness = 3 mm, FOV = 300 × 300 mm, and number of slices = 75) was acquired for attenuation correction purposes. PET data were reconstructed using the TrueX (HD-PET) algorithm and smoothed with a 2-mm Gaussian kernel with scatter correction.

During follow-up visit, participants underwent Tau PET imaging with 18F-MK-6240 tracer in a Siemens Biograph64 mCT/PET scanner (dynamic, 3D acquisition mode, 6 dynamic frames within 30 min). Brain PET image acquisition started 80–100 min after the bolus injection of the 18F-MK-6240 tracer (5 mCi dose). An accompanying structural CT scan was acquired as well. PET images were reconstructed using an iterative algorithm with a voxel size of 1 × 1 × 2 mm.

Data acquisition and preprocessing in the ADNI study

In the ADNI-3 study, MRI scanner protocols and parameters can be found in (https://adni.loni.usc.edu/data-samples/adni-data/neuroimaging/mri/mri-scanner-protocols/). Briefly, MR images were acquired with an ADNI standardized pulse sequence at various sites using 3 Tesla scanners. Anatomical T1-weighted structural image was acquired using MPRAGE (TR/TE = 2300/2.96 ms; FOV = 240 × 256 mm; matrix size = 240 × 256 voxels; voxel size = 1 × 1 × 1 mm; 208 sagittal slices). Diffusion MR images were acquired with spin-echo echo-planar diffusion-weighted sequences. Most participants' data were acquired with a single shell sequence (TR/TE = 7200/56 ms, matrix size = 232 × 232 mm, voxel size = 2 × 2 × 2 mm, 80 axial slices, b = 1000 s/mm^2 with 48 gradient directions, and 7 volumes with b = 0 s/mm^2). However, sequence parameters are different for different scanners; please see details in the Supplementary Materials. To employ Aβ PET imaging, participants were administered an intravenous catheter of [^{18}F]Florbetapir (AV45, 10 mCi ± 10% dose). Then, a low-dose CT image for PET was acquired, followed by a brain PET image acquisition that started 50–70 min after the injection (dynamic, 3D acquisition mode, 4 × 5-min frames over 20 min). The same structural data preprocessing conducted on the CogRes/RANN study participants was performed on ADNI data, including the FreeSurfer pipeline, brain parcellation with the Schaefer atlas, and subcortical ROIs delineation with FreeSurfer. However, a newer version of the FreeSurfer (v7.0) was used in ADNI data preprocessing.

PET regional amyloid-β and Tau SUVR analysis

An in-house-developed automatic quantification approach was used to analyze Aβ PET scans[51]. Briefly, four dynamic PET frames were aligned to the first frame using rigid-body registration and averaged to create a static PET image. This static PET image was then co-registered with the accompanying CT scan to generate a composite image. Then, each participant's structural T1w image was registered to the composite PET-CT image (rigid-body registration with cost function as mutual information). ROIs and the cerebellar gray matter mask were transformed into the static PET image space. Regional PET data were extracted from these 200 cortical ROIs, and PET signals in the subcortical regions were not included in the analysis. Lastly, the standardized uptake value (SUV) was calculated for each ROI and was normalized to the value in the gray-matter cerebellum mask to derive SUVR. The same amyloid-β SUVR analysis was performed on ADNI PET imaging data. The same approach was used to analyze Tau PET scans: the static PET image was co-registered to the CT scan to generate a composite PET-CT image, and FreeSurfer regional masks, temporal lobe mask, and cerebellar gray matter mask were transformed into the static PET image space. Regional Tau PET SUVRs were computed by normalizing the regional SUV with the average uptake value in the cerebellar gray matter region.

fMRI preprocessing and functional connectivity analysis

An in-house-developed method was used to derive functional connectivity from resting-state fMRI data[52]. First, slice timing correction was carried out with Fourier-space time-series phase-shifting by using the FSL software package (version 6.0.4)[53]. Then, motion correction was performed using rigid-body registrations on all the volumes in reference to the first time point volume[54]. An fMRI reference image was created by averaging all the aligned EPI volumes. Frame-wise displacement (FWD) was then calculated for each subject[55], using the six motion parameters and the root mean square difference (RMSD) of the realigned fMRI signal between consecutive volumes. Scrubbing was performed to exclude fMRI-contaminated volumes (if FWD exceeded 0.5 mm or RMSD surpassed 0.3%). Contaminated volumes were replaced with new ones generated through linear interpolation of adjacent volumes. Next, band-pass filtering was carried out with cut-off frequencies of 0.01 and 0.08 Hz, using the FSL software package with nonlinear high-pass and Gaussian linear low-pass. Finally, after motion correction, scrubbing, and temporal filtering, we regressed out the FWD, RMSD, white matter signals from both hemispheres, and lateral ventricular signals from the preprocessed fMRI data. No global signal regression was applied. The averaged fMRI time-series signals were extracted from the 200 cortical ROIs. Then, functional connectivity matrices were calculated with Pearson's correlation, and the correlation matrices were Fisher z-transformed to generate normalized connectivity matrices with the diagonal set to zeros. QC was performed based on ref. 56, by computing the variance of the mean signal within each ROI. Participants were excluded if at least one region had zero (or very low) variance.

DTI preprocessing and structural connectivity analysis

Structural connectivity was generated following the procedures outlined in Basic and Advanced Tractography (BATMAN)[57] and using the MRtrix3 software[58]. First, diffusion MRI data were preprocessed with steps of denoising[59], Gibbs' ringing artifact correction[60], EPI geometric distortion correction[61], eddy current and motion distortion correction[62], bias field correction[63], and brain mask estimation. Then, response functions for white matter, gray matter, and cerebrospinal fluid were estimated, followed by intensity normalization to correct global intensity differences. Whole-brain streamlines were generated through anatomically constrained tractography, creating 10 million streamlines per subject. The tractograms were then filtered using the spherical-deconvolution informed filtering of tracks to improve streamline density distribution. Finally, structural connectivity matrices were created using the predefined 214 cortical and subcortical ROIs extracted from the Schaefer atlas and FreeSurfer segmentation. The streamline count was normalized with regard to the inverse of the node volumes. The connectivity matrices were symmetrized, and the diagonal was set to zero. QC was performed based on ref. 56, specifically, we computed QC measures for connectome matrix density, number of connected components, and reconstructed streamlines. Participants were excluded if they had more than one connected component, or either matrix density or number of streamlines fell outside three standard deviations from the group mean. The following analyses included only the structural connectivity of the 200 cortical ROIs.

Network-based amyloid-β pathology (NAP) measures

As shown in Fig. 1, the proposed connectivity-weighted NAP score was computed as the matrix product of regional Aβ deposition A_i in region $i = 1,\ldots, N$ ($N = 200$ regions of interest) and connectivity matrix C_{ij} between region i and j ($j = 1,\ldots, N$), denoted as: $A_i \times (C_{ij} + I)$. The connectivity-weighted (CW) NAP deposition at region i quantifies not only the regional Aβ deposition A_i, but also Aβ deposition in all other regions j ($j = 1,\ldots, N$) connected to region i, weighted by the strength of their structural or functional connectivity: $\mathrm{NAP}_i^{CW} = A_i + \sum_j^N C_{ij}A_j$. The proposed centrality-scaled (CS) NAP score was quantified by a Hadamard product of regional Aβ deposition A_i in region $i = 1,\ldots, N$ (N regions of interest) and the centrality of region i in the connectivity matrix C_{ij}, denoted as: $\mathrm{NAP}_i^{CS} = A_i \odot (\sum_j^N C_{ij})$. The centrality-scaled NAP score quantified regional Aβ deposition A_i, and scaled it by its centrality regarding the whole connectivity matrix C_{ij}. In both NAP scores, the connectivity matrix can be generated either using structural diffusion data or functional MR data, denoted as C_{ij}^S or C_{ij}^F, respectively.

Cross-validated predictive modeling

CPM was adapted to evaluate the Aβ-cognition relationship. CPM used either structural or functional connectivity patterns to predict individual differences in behavior and cognition. Instead of using connectivity as brain measurements, we used either regional SUVR or NAP measures of brain amyloid to predict longitudinal cognitive decline. Because the leave-one-out approach has been shown to introduce biased estimates, repeated random splits of K-fold cross-validation modeling were chosen as a more stable approach[64,65]. We employed 500 repetitions to account for the impact of random train-test data partitions, and the median prediction performance was reported. The cross-validated predictive modeling included four steps, as shown in Fig. 2: (1) Participants splitting: subjects were randomly split into K-fold ($K = 15$ was chosen in this study, see Supplementary Materials for details), including a training set and a test set.

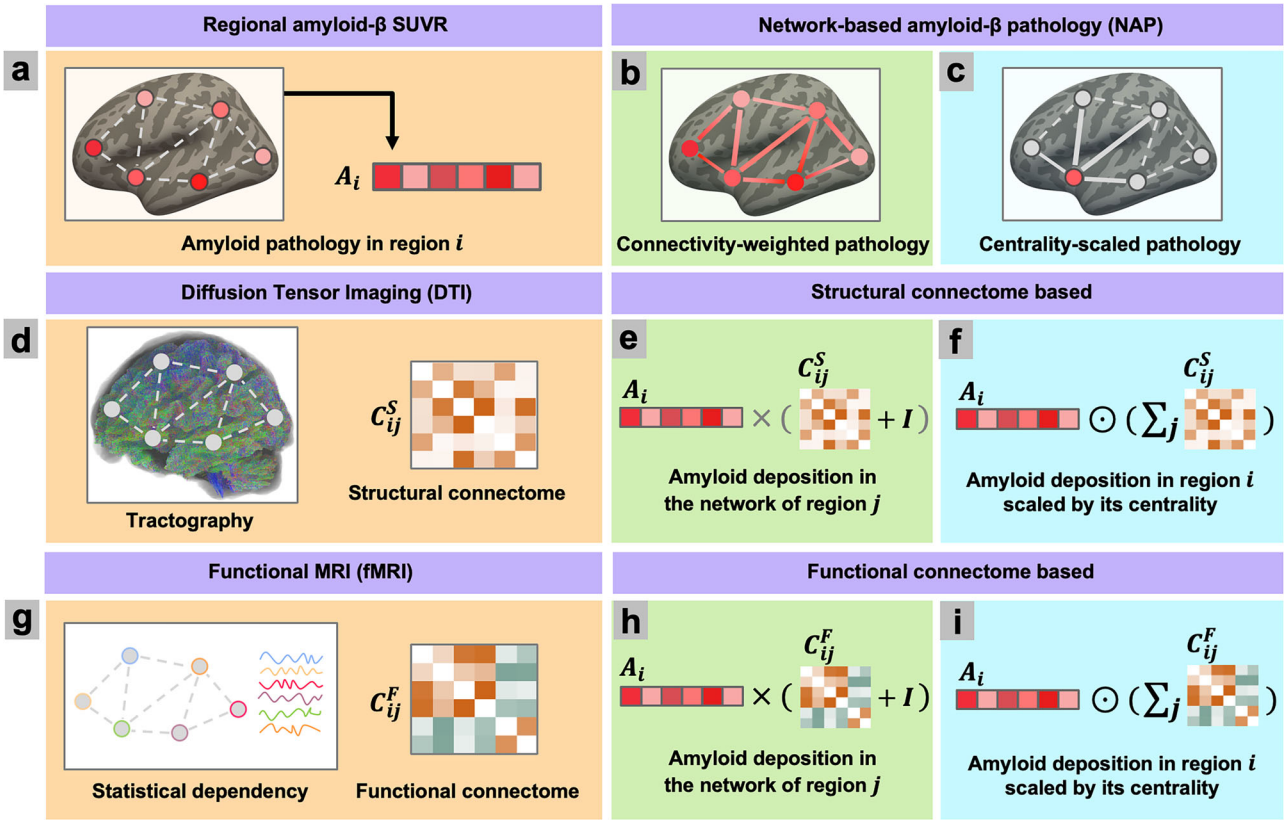

Fig. 1 | Regional amyloid-β standardized uptake value ratio (SUVR) and network-based amyloid-β pathology (NAP). In addition to regional SUVR, the proposed NAP scores incorporate connectome information by using either a connectivity-weighted or centrality-scaled approach. Here, we show a six-region toy network. **a** Illustration of regional SUVR deposition A_i in region i ($i = 1,\ldots, 6$). **b** Connectivity-weighted NAP score quantified the influence of amyloid-β (Aβ) deposition within the connected networks. **c** Centrality-scaled score quantifies the Aβ deposition in the region and scaled it by its centrality in the connectome. Network connectome information can be generated based on either structural connectome (SC) (**d**) or the functional connectome (FC) (**g**). **d** SC is derived from tractography on diffusion tensor imaging data, where the SC matrix was denoted as C_{ij}^S. **e** SC-based connectivity-weighted NAP score of region j quantifies both the Aβ in region j and a weighted sum of Aβ in all other regions based on connectivity values, where the whole process was denoted as matrix multiplication of $A_i \times \left(C_{ij}^S + I\right)$. **f** SC-based centrality-scaled NAP score of region i is quantified by a Hadamard product of regional SUVR measure and connectivity centrality $A_i \odot (\sum_j^6 C_{ij}^s)$. **g** FC is computed from statistical dependency on functional MRI data. For the connectivity-weighted (**h**) and centrality-scaled pathology (**i**), FC-based NAP scores are computed in the same way as the SC-based approach, but with FC denoted as C_{ij}^F.

In the training set, as shown in Fig. 2b, we first regressed out covariates related variability (age, sex, education, corresponding baseline cognition, and hemispherical mean cortical thickness) from the longitudinal cognition change. This covariate-related variability was also removed from the test set using the same coefficient weights from the training set. (2) Feature selection: in the training set, the pathology measure (either regional or network-based amyloid) of each ROI was correlated with the longitudinal cognitive change (residual from the first step). Features/regions were selected showing a strong negative correlation with an uncorrected p value less than 0.05 (because elevated pathology deposition was expected to associate with severe cognitive decline). (3) Model training: In the training set, the sum of selected features was regressed against residual cognitive change to obtain model weights. (4) Model validation: In the test set, the sum of the features in the same selected ROIs and the model weights from step (3) were used to compute predicted cognitive change. In the loop of each hold-out fold, the same processes were performed, resulting in a predicted cognitive change value for each participant. Lastly, statistical analyses were performed to compare the predicted and the actual cognitive change values in the collection of all hold-out samples. The whole process of cross-validation was repeated 500 times. An Aβ neuropathological signature pattern was derived for each of the pathology measures input. Regions in the pattern were identified if the regional features were selected 95% times during the repetition of cross-validation.

Statistical analysis of predictive model performance

For each model, two metrics were computed to evaluate the predictive performance, including Pearson's correlation coefficient and root mean squared error (RMSE) as $\hat{\sigma} = \sqrt{\frac{\sum(y-\hat{y})^2}{n}}$, where y and $\hat{y}$ are the actual and predicted cognitive decline scores, respectively, and n denotes the sample size. To compare the predictive performance across pathology models, the train-test partitions in the 500 times repetition were kept the same for each model. Each model was then compared to the performance of the regional SUVR measure, which served as the reference model. We report the median correlation coefficient, the difference in correlation coefficient to the reference model, and the ratio of RMSE over the reference model. Because the absolute value of RMSE can be difficult to interpret across models, we calculated the *Ratio*, which quantifies the RMSE of each model compared to the regional SUVR reference model and was computed as the RMSE of the model divided by that of the reference model. Between each model and the regional SUVR reference model, an empirical one-sided signed test was performed on the histogram of the difference in correlation coefficient, and p values were reported.

External generalizability analysis on the ADNI dataset

As evidenced in the existing literature[13–17], the Aβ-cognition relationship has consistently been observed in the episodic memory domain and global

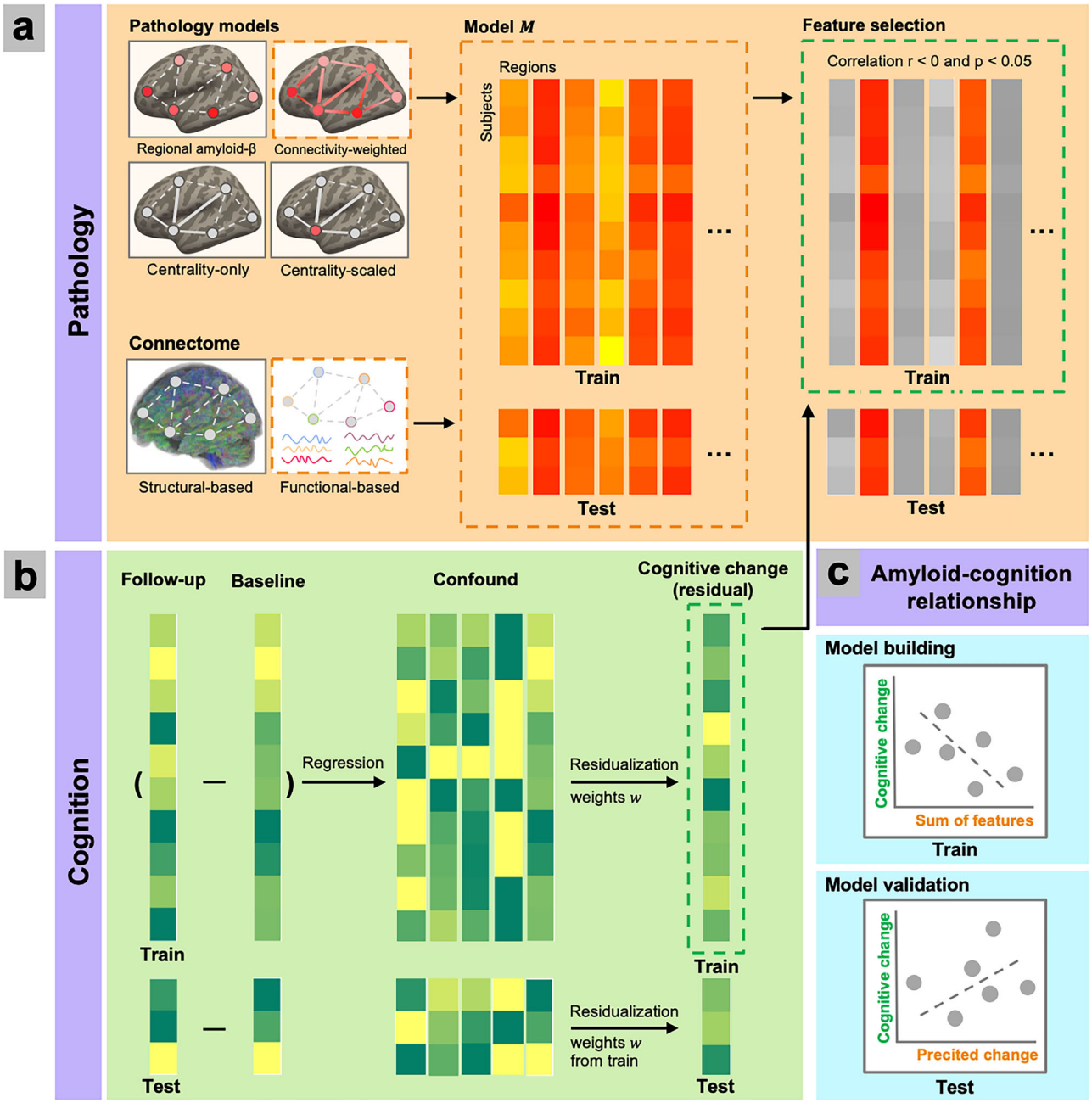

Fig. 2 | Cross-validated predictive modeling analysis overview. The figure illustrates an example of using connectivity-weighted network-based amyloid-β pathology (NAP) with a functional-based connectome. **a** *Feature selection on the input of pathology models and connectome*. Regional standardized uptake value ratio (SUVR) or NAP (either connectivity-weighted or centrality-scaled) can be used as input. Regional SUVR measures do not need the input of connectome information, and the centrality-only model has only connectome information (serving as a benchmark for NAP measures). A feature is selected if it shows a negative correlation with the cognitive change residual score at an uncorrected $p < 0.05$ in the training set. **b** *Computation of longitudinal cognitive change scores*. Subjects are randomly split into a training set and a test set. In the training set, we regress out covariate confounds from the longitudinal cognitive change. The covariate-related variability is also removed from the test set using the same weights. **c** *Regression of selected amyloid pathology features in the train set and prediction of cognitive decline in the test set*. The sum of selected features is regressed against cognitive change residual scores from the training sample to obtain model weights. The obtained weights are then applied to the features from the test set to predict cognitive decline scores, which were then compared to actual scores to evaluate model prediction performance.

cognition. Therefore, in the generalizability external validation, we tested the Aβ neuropathological signatures derived from the internal CogRes/RANN dataset on the following neuropsychological assessments in the ADNI-3 dataset: (1) ADNI-Mem; (2) ADNI-GCog; (3) dMemory. Using the same approach as that used for the cross-validated predictive model analysis, the residual of the longitudinal cognitive change (follow-up minus baseline) was computed by regressing out covariates, including age, sex, education, hemispherical mean cortical thickness, and the corresponding baseline cognition. Because ADNI-3 participants had a large variability in the time interval between baseline and follow-up cognition, this time interval variability was included as an additional covariate.

The same structural T1-weighted MR data analyses were applied to the ADNI-3 dataset, including brain parcellation pipelines and cortical thickness estimation with FreeSurfer. However, a newer version of the FreeSurfer (v7.0) was used. Manual inspection and editing were conducted by a technician to ensure quality control on cortical surface reconstruction and white and gray matter borders delineation. The diffusion MR data used for each participant were selected based on the closest time interval between

data collection and the baseline neuropsychological assessments. Then, the same preprocessing and structural connectome procedures were performed to derive structural connectivity in the ADNI-3 cohort. However, the pipeline was slightly adjusted for three participants due to the use of a different acquisition sequence involving a multi-shell scheme.

For the external generalizability validation on the Aβ neuropathology signature, we extracted the features (regional SUVR, connectivity-weighted NAP, or centrality-scaled NAP values) in the corresponding signature pattern for each pathology model. Then, the sum of features was used to predict cognitive decline, using the same weights estimated on the internal dataset. To evaluate the performance, Pearson's correlation was calculated between the predicted values and the actual cognitive decline residual scores in each of the ADNI cognition (ADNI-Mem, ADNI-GCog, or dMemory). Additionally, we tested whether the observed relationship reflects general Aβ deposition in the brain, rather than being specific to the distinct signature patterns that are characteristic of future cognitive decline. To test such regional specificity, we conducted a control analysis where we randomly selected a set of ROIs, ensuring that the number of ROIs matched those identified in the Aβ neuropathological signature. Then, for each iteration, we used the features from this randomly selected set of ROIs to predict cognitive decline, and we recorded the correlation coefficient between the predicted values and the actual cognitive decline scores. This process was repeated 500 times, resulting in a distribution of the correlation coefficients. Lastly, the observed relationship in the signature ROIs was compared to this control analysis distribution, and the p values in the regional specificity randomization test were reported. The p value was calculated as the proportion of randomizations that produced a correlation greater than or equal to the observed prediction correlation.

Statistics and reproducibility

In the CogRes/RANN cohort, we included 85 cognitively normal older adults in this study. We first tested associations between regional baseline Aβ-PET SUVR and longitudinal cognitive decline using Spearman partial correlations, controlling for age, sex, education, baseline cognition, and hemispheric mean cortical thickness. The significance level was set at $p < 0.05$, and multiple comparisons were corrected using false-discovery rate (FDR; $q < 0.05$). Next, in the cross-validated predictive modeling, the significance of model performance was assessed by permutation testing (500 times shuffling). The Aβ-PET regional SUVR model was used as the reference model, and between-model performance differences were evaluated with a one-sided sign test on the distribution of correlation differences across cross-validation repetitions. External validation was performed in the independent ADNI cohort ($n = 72$ cognitively normal participants). Specifically, we tested whether features from the same signature ROIs (derived in the CogRes/RANN cohort) provided superior prediction performance of prospective cognitive decline in ADNI. This regional specificity was assessed via a randomization test, comparing the performance of the signature ROI set with a null distribution of performance from 500 size-matched random ROI sets.

Results

The interval between baseline and follow-up neuropsychological assessments ranged from 3 to 7 (4.51 ± 0.68, mean ± SD; SD, standard deviation) years. A subset of the neuropsychological assessments was used to examine participants' cognition in four domains: episodic memory, vocabulary, processing speed, and fluid reasoning. Cognitive composite scores for each cognitive domain were generated and normalized by subtracting the baseline sample mean and dividing by the baseline sample standard deviation. An average of the four z-scores of all four cognitive domains was calculated to yield a global cognitive score. More details of neuropsychological assessments are described in Table S1. Overall, participants showed a decline in global cognition (Fig. S2). However, it is important to note that these changes reflect subclinical variation, and all participants remained within the cognitively normal range at follow-up, as defined by the DRS ≥ 130.

As illustrated in Fig. S1, the average global amyloid SUVR of the CogRes/RANN participants in this study was 1.16 with a standard deviation of 0.09, and 2 participants were considered amyloid positive based on a cut-off of 1.40, where previous PET imaging studies with Florbetaben tracer have identified cut-off values as 1.34[66], 1.40[67], or 1.48[68]. Consistent with other studies on cognitively normal individuals, global amyloid SUVR in our sample tends to follow a unimodal but right-skewed distribution[69]. Based on this distribution of global amyloid and the methodological challenges to dichotomize amyloid status at the regional level, in this study, we treat regional amyloid as a continuous variable to preserve its variability.

Association of global and regional Aβ with future cognitive decline

As linear statistical modeling is commonly used to study the Aβ-cognition relationship[14,17,23,70], we first performed a similar statistical association analysis before employing the cross-validated predictive modeling. The correlations between baseline Aβ pathology (PET imaging with Florbetaben tracer) and prospective decline in each cognitive domain and in global cognition were assessed using Spearman partial correlation, controlling for age, sex, education, baseline cognition, and hemispherical mean cortical thickness. When using global SUVR of Aβ pathology, no significant relationships to cognition were observed (reasoning: $r = 0.1426$; $p = 0.2012$; memory: $r = 0.1240$; $p = 0.2671$; vocabulary: $r = 0.1957$; $p = 0.0840$; processing speed: $r = -0.0577$; $p = 0.6067$; global cognition: $r = 0.0919$; $p = 0.4207$). Next, we performed similar correlation analyses for each regional Aβ measure. The significance level was set as $p < 0.05$ with FDR multiple-comparison correction for a total of 200 cortical regions (Schaefer Atlas). We found significant relationships for the vocabulary cognitive domain, but not for reasoning, memory, processing speed, nor global cognition. Higher baseline regional SUVR in the left hemispherical extrastriate cortex (part of the central visual network) was significantly related to greater decline in vocabulary ($r = -0.4044$, FDR-corrected $p < 0.0438$; uncorrected $p < 0.0002$).

The non-significant results observed may be attributed to the use of a less sensitive non-parametric method, which was employed to accommodate the non-normal distribution of Aβ pathology[14]. Although weak but significant associations between Aβ deposition and future cognitive decline have been well-established in the literature[13–17], the results of statistical association analyses can be influenced by the complexity of the statistical model and the sample size. Given that the Aβ-cognition relationship was evaluated using within-sample correlations, the results might not predict such a relationship for the new individuals, and are not adequate to support predictive validity of early Aβ on cognition[64,71]. To improve generalizability in the findings of the amyloid-cognition relationship, we next used cross-validated models.

Baseline regional Aβ predicts subsequent cognitive decline in global cognition

As Aβ deposition has been reported to yield the largest effect size on global cognition[15], we focused on this relationship. We employed a cross-validated predictive modeling approach, where a framework was adapted from CPM[30–32]. Briefly, participants were randomly split into training and test partitions (Fig. 2a, b). We regressed out covariate confounds from the longitudinal cognitive change in the training set, and the covariate-related variability is also removed from the test set using the same weights. Next, for the amyloid-cognition relationship, feature selection and model building were performed on the training set by Spearman correlation and linear modeling, respectively (Fig. 2a, c). Lastly, model predictive performance was evaluated on the correlation coefficient between predicted cognitive decline score and the actual cognitive change (cognition was assessed as residual value controlling covariates; Fig. 2b). As repeated k-fold cross-validation has proven to produce less biased estimation than the leave-one-out approach[65], we used a 15-fold cross-validation modeling, and the random partitions of train and test sets were repeated 500 times to obtain a stable result (details of cross-validation fold number selection are in Supplementary Materials).

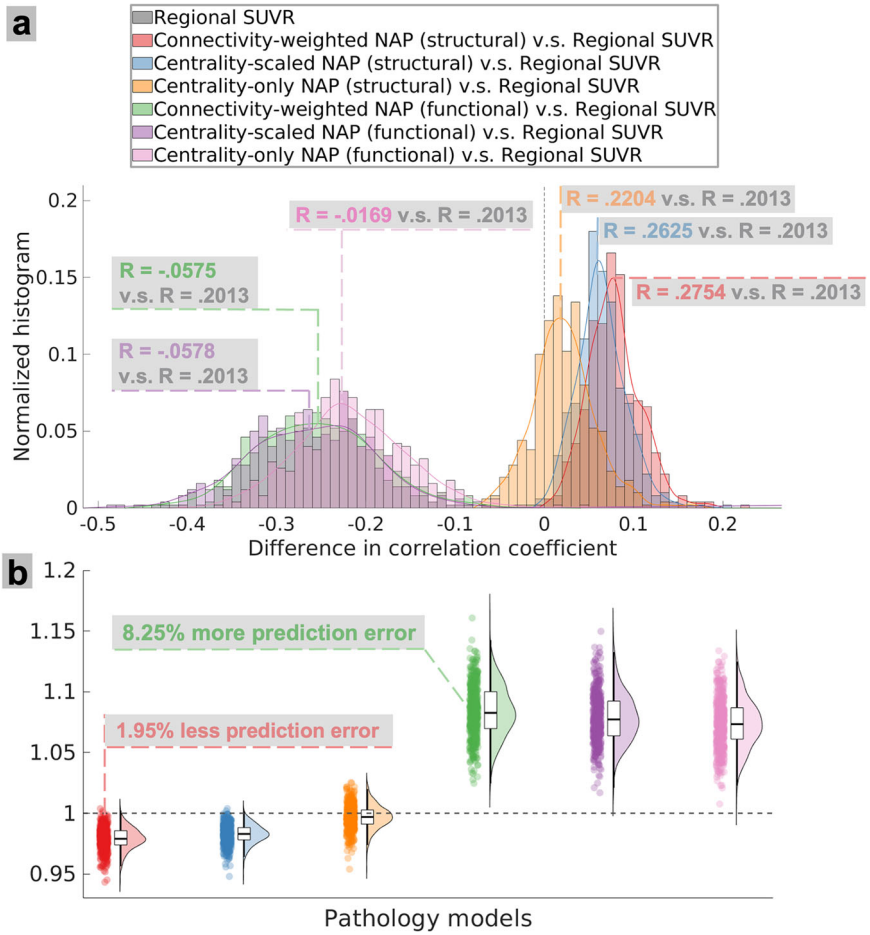

Fig. 3 | Performance of cognitive decline prediction using different pathology models across cross-validation repetitions. a Distributions of differences in correlation coefficients between predicted and actual cognitive decline scores across different pathology models. Prediction performance was compared across cross-validation repetitions with the regional standardized uptake value ratio (SUVR) model as the reference. Incorporating structural connectome (SC) with connectivity-weighted network-based amyloid-β pathology (NAP) achieved the highest performance, and outperformed the prediction performance of regional SUVR measures. **b** Comparison of the *ratio* of root mean squared error (RMSE) performance between pathology models. Compared to regional SUVR measures, connectivity-weighted NAP measure of SC had smaller RMSE, whereas connectivity-weighted NAP measures of functional connectome (FC) had higher RMSE. The analysis included seventy-seven participants for whom all data were available.

The predictive performance was evaluated as the median value across repeated iterations. First, we performed the cross-validated predictive modeling on regional SUVR measures (Fig. 2a) to predict cognitive decline in global cognition. The same predictive modeling can be fitted to other pathology models, such as NAP, incorporating either structural or functional connectome (see "pathology models" in Fig. 2a). For regional SUVR measures, a median correlation coefficient $R = 0.2013$ was found between the predicted cognitive decline in global cognition and the actual values. To test its significance level, we generated an empirical null distribution by shuffling the cognitive decline variable 500 times (the covariates were ordered the same each time as the cognitive decline variable to keep correspondence). The p value was calculated as the proportion of permutations that were greater than or equal to the actual correlation. We found that baseline regional SUVR measures significantly predict subsequent cognitive decline in global cognition ($p < 0.0419$), indicating that the observed correlation coefficient $R = 0.2013$ is significantly higher than the amyloid-cognition relationship observed by chance.

Connectome-based modeling of the Aβ improves prediction of subsequent cognitive decline

Here, we performed the same cross-validated predictive modeling approach (Fig. 2) on connectome-based modeling of the Aβ (Fig. 1). In addition to the regional Aβ deposition (Fig. 1a), we examined how the measures of Aβ deposition within individualized brain connectivity networks contribute to subsequent cognitive decline. Thus, we developed NAP scores by leveraging the connectivity profile (either structural or functional) of each ROI (Fig. 1b, c). As shown in Fig. 1e, h, the proposed connectivity-weighted NAP scores quantified the influence of Aβ deposition within the connected network associated with each ROI, where the NAP measure of each region quantifies not only the regional Aβ deposition in the region, but also Aβ in all other regions connected to this region, weighted by its connection strength to the region. A simpler version of NAP scores, i.e., centrality-scaled NAP, was also developed to quantify only the regional Aβ deposition in the region, and it is scaled by the centrality (nodal strength) of the region in the connectivity matrix (Fig. 1f, i). The rationale for such measures is that highly connected regions are crucial for cognitive functioning, and Aβ-related disruption of such regions may lead to more distributed effects on brain dynamics, and subsequently more severe cognitive decline[72]. Incorporating connectome information into pathology measures allowed us to identify network-based neuropathological patterns that might be predictive of cognitive decline. NAP measures could potentially uncover cognition-relevant pathological disconnection patterns. Specifically, we first obtained subject-specific structural and functional connectivity between each pair of ROIs through tractography and resting-state fMRI data, respectively (Fig. 1d, g). Then, we adopted the same cross-validated predictive modeling approach to evaluate and compare the performance of regional SUVR and NAP measures, and additional models with only connectome centrality measures (no Aβ pathology information) were included as a benchmark for comparison.

To compare the predictive performance across pathology models, the train/test partitions for the cross-validation repetitions were kept the same for each model. Predictive performance was assessed by comparing predicted and actual cognitive decline scores with the median correlation coefficient and the ratio of RMSE (denoted as *Ratio*). As shown in Fig. 3a, b, four different predictive models were built based on different network-based measures (connectivity-weighted or centrality-scaled measures) of brain connectome and pathology, and were all compared to the predictive model purely based on regional amyloid SUVR. The performance difference in the correlation coefficient and the *Ratio* was reported. In addition, two

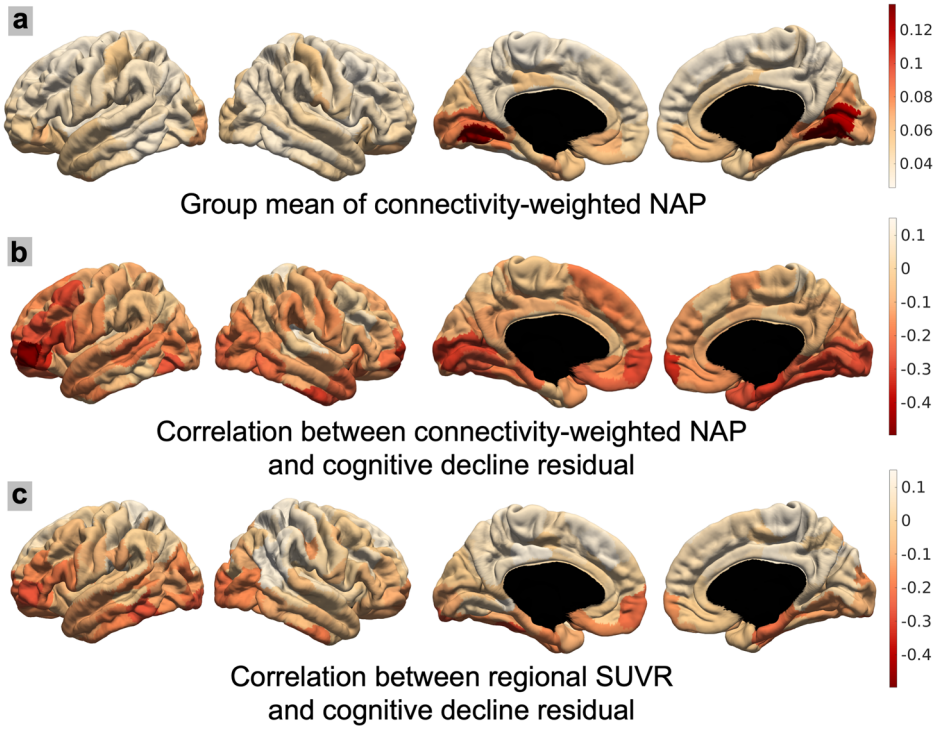

Fig. 4 | Regional standardized uptake value ratios (SUVR) and network-based amyloid-β pathology (NAP) maps. a Group averaged structural connectome (SC) connectivity-weighted NAP scores. **b** Correlation coefficient between cognitive decline and SC connectivity-weighted NAP scores across cortical regions of interest (ROIs) (Spearman partial correlation, controlling for age, sex, education, baseline cognition, and hemispherical mean cortical thickness). **c** Correlation coefficient between cognitive decline and regional SUVR scores across cortical ROIs. NAP scores have higher values in basal cortex regions (**a**). Individual variability in NAP scores in basal cortex regions and the left dorsolateral prefrontal cortex scales with cognitive decline (**b**), showing a stronger negative correlation with subsequent cognitive change compared to regional SUVR scores (**c**). The analysis included seventy-seven participants for whom all data were available.

predictive models were also built based on the connectome information only (centrality-only measures). To test the significance level of predictive performance, the same permutation procedure was employed by shuffling the cognitive decline variable. Regional SUVR measures predicted cognitive decline with a median correlation coefficient $R = 0.2013$, which is significantly higher than the amyloid-cognition relationship observed by chance ($p < 0.0419$). Structural connectivity information seems to be predictive of cognitive decline by itself, with centrality-only measures showing significant performance (median $R = 0.2204$, permutation $p < 0.016$). However, the prediction performance was the highest for the NAP measures when combining the information from both regional SUVR and structural connectome information. Structural connectivity-based NAP measures also significantly predicted cognitive decline (connectivity-weighted NAP: median $R = 0.2754$, permutation $p < 0.008$; centrality-scaled NAP: median $R = 0.2625$, permutation $p < 0.010$). However, functional connectivity information itself had a worse performance compared to regional SUVR, with a non-significant performance using centrality-only measures (median $R = -0.0169$, permutation $p > 0.4451$). Incorporating functional connectome information into the NAP measures made the predictive performance worse than regional SUVR (connectivity-weighted NAP: median $R = -0.0575$, permutation $p > 0.5549$; centrality-scaled NAP: median $R = -0.0578$, permutation $p > 0.5349$). Additionally, we further compared the performance of structural connectome-based NAP and regional SUVR measures. As shown in Fig. 3a, the performance of NAP measures is significantly higher than that obtained by regional SUVR measures, with a difference in correlation coefficients significantly higher than zero (connectivity-weighted NAP: $p < 0$; centrality-scaled NAP: $p < 0.006$). The performance of centrality-only measures is higher than that obtained by regional SUVR measures, but the difference is not significant ($p > 0.2440$).

In an additional analysis, to identify and visualize the brain ROIs contributing most to the observed relationships between pathology and cognition, we conducted a Spearman partial correlation analysis between the pathology features in each ROI and cognition change, controlling for age, sex, education, baseline cognition, and hemispheric mean cortical thickness. As shown in Fig. 4a, structural connectome-based connectivity-weighted NAP scores had higher values in the basal cortical regions of the temporal and occipital lobes compared to other brain regions. These regions, along with the medial prefrontal cortex and left dorsolateral prefrontal cortex, exhibited a stronger negative correlation with longitudinal cognitive change than other areas of the brain (Fig. 4b). Furthermore, NAP scores showed a more pronounced negative correlation with longitudinal cognitive changes compared to regional SUVR scores (Fig. 4c). Similar patterns were observed for the centrality-scaled NAP scores (Fig. S3). Figure 4b, c illustrate that individuals with higher levels of amyloid pathology in the highlighted regions (shown in red) tend to experience faster cognitive decline, whereas individuals with lower amyloid burden in these regions tend to show slower cognitive decline.

While these results (Fig. 3a, b) were based on unthresholded connectome matrices, the overwhelming number of connections might make it difficult to extract meaningful information. Thus, we additionally tested whether keeping only meaningful connections above a proportional threshold will improve the performance of functional connectivity-based NAP measures. A proportional threshold approach was used as it has been shown to give more stable network measures than an absolute threshold approach[73]. As shown in Fig. S4a, a stricter threshold did improve the predictive performance with lower *Ratio* values compared to the performance of regional SUVR. However, even the best performance model with a threshold of keeping the top 2% connections (connectivity-weighted NAP: median $R = 0.0557$; centrality-scaled NAP: median $R = 0.0620$) still performed worse than regional SUVR measures (Fig. S4b).

Forward application of identified neuropathological signatures predicts future cognitive decline in an external dataset

Here, we aimed to perform external validation on the selected features in the cross-validated predictive modeling analyses (Fig. 2). This data-driven approach could identify neuropathological patterns of either regional or network-based Aβ deposition that maximally predict future cognitive decline. To illustrate the results of feature selection in the cross-validated predictive modeling, Fig. 5 presents brain ROIs where pathology measures are predictive of future cognitive decline, by using regional SUVR measures (Fig. 5a), connectivity-weighted NAP measures (Fig. 5b), or centrality-scaled NAP measures (Fig. 5c). These regions were identified if the features were selected for 95% of the iterations in cross-validation. As shown in Fig. 5, the Aβ neuropathological signatures identified regions located in the basal

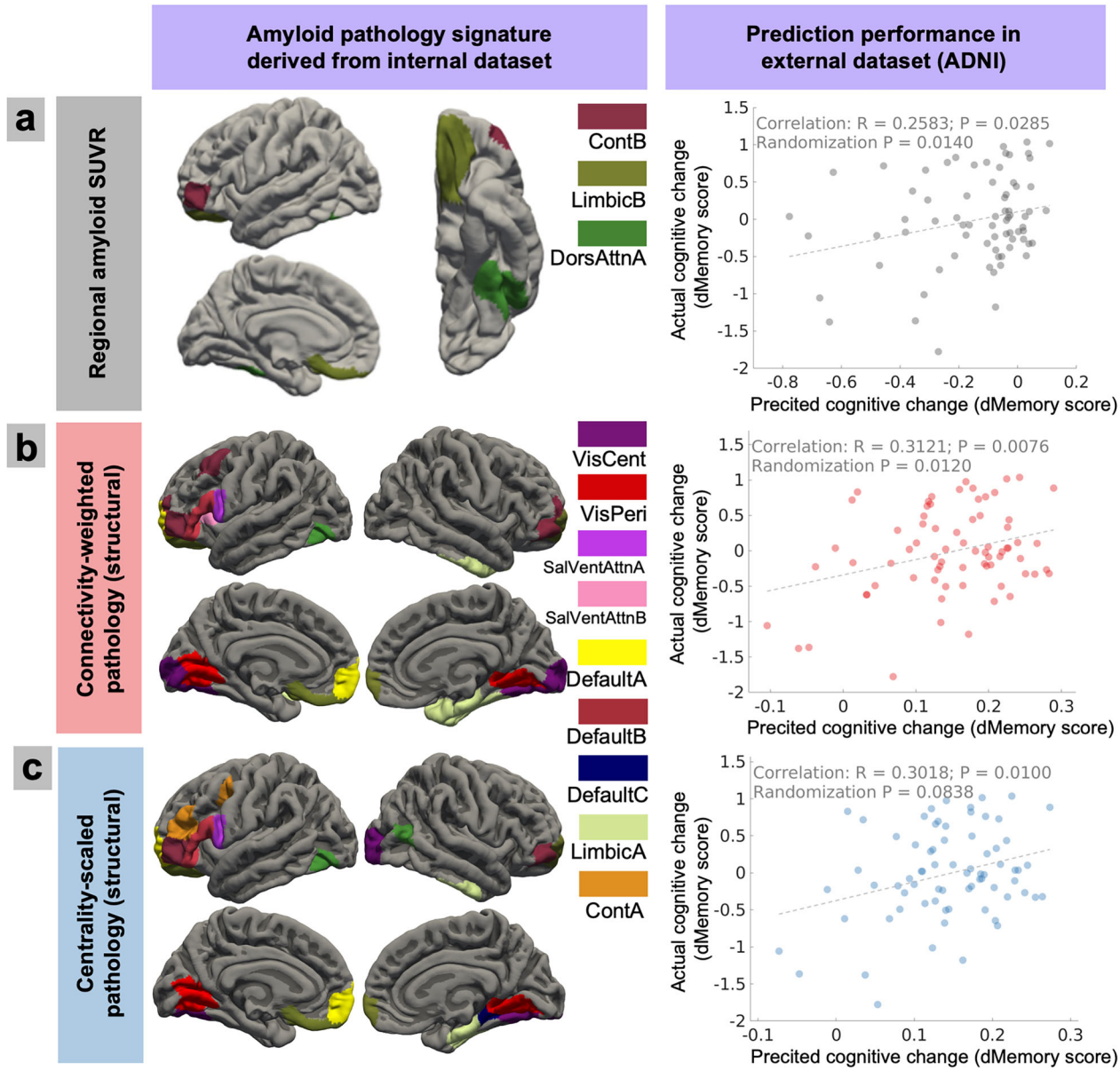

Fig. 5 | The amyloid-β (Aβ) neuropathological signatures of future cognitive decline and external validation. a Regions of interest (ROIs) whose regional Aβ standardized uptake value ratio (SUVR) measures were identified as features of future cognitive decline. This pattern of pathology signature was derived from the internal CogRes/RANN dataset. In external validation, features within the same ROIs pattern of ADNI participants were used to predict cognitive decline in dMemory, and subsequently compared to the actual decline score. The predicted cognitive change significantly correlated with the actual score (Pearson correlation; two-sided), and the relationship is significantly higher than the results obtained by random ROI selection (Randomization test; one-sided), demonstrating regional specificity. **b** Results of Aβ neuropathological signatures using connectivity-weighted network-based Aβ pathology (NAP) measures. **c** Results of Aβ neuropathological signatures using centrality-scaled NAP measures. The color indicates the network label of each ROI based on the Schaefer atlas. The analysis included seventy-two participants for whom all data were available. Cont: cognitive control network, DorsAttn: dorsal attention network, VisCent: visual central network, VisPeri: visual peripheral network, SalVentAttn: salience/ventral attention network, Default: default mode network.

portions of the frontal, temporal, and occipital lobes, consistent with the early-stage Aβ deposition patterns reported in other PET and autopsy studies[26,74]. The exact region labels and location are reported in Supplementary Data 5.

We first validated the signature pattern in the same internal CogRes/RANN dataset. Features in the signature pattern were used to predict cognitive decline, and subsequently were related to the actual cognitive decline score (residual controlling age, sex, education, baseline cognition, and hemispheric mean cortical thickness) in global cognition, as well as in each cognitive domain. The predicted score significantly correlated with cognitive decline in both global cognition and episodic memory, but not in fluid reasoning, vocabulary, or processing speed (Results shown in Table S2). Within the same dataset, the results indicate that the predictive validity of Aβ pathology in global cognition is mostly driven by its relationship to episodic memory. This is consistent with literature showing the robust relationship between Aβ deposition and cognitive decline in episodic memory[13–17]. Next, we sought to validate the derived Aβ neuropathological signatures' relationships to cognitive decline using an external dataset. We used the ADNI dataset (adni.loni.usc.edu) and, based on the findings using the internal CogRes/RANN dataset, we focused on the cognitive decline in global cognition and episodic memory. Three cognition scores were extracted: (1) ADNI memory score (ADNI-Mem)[41]; (2) ADNI global

Table 2 | Model performance of amyloid-β neuropathological signatures on the ADNI external dataset validation

Cognitive decline measures	Regional amyloid-β (Aβ) SUVR	Connectivity-weighted network Aβ pathology	Centrality-scaled network Aβ pathology
ADNI global cognition score	*r = 0.1894; p = 0.0379 (*)*	*r = 0.1902; p = 0.4271*	*r = 0.1858; p = 0.6467*
ADNI memory score	*r = 0.1456; p = 0.1836*	*r = 0.1264; p = 0.0978*	*r = 0.1188; p = 0.1497*
dMemory score	*r = 0.2583; p = 0.0140 (*)*	*r = 0.3121; p = 0.0120 (*)*	*r = 0.3018; p = 0.0838*

Here, we report the Pearson correlation (*r* value) between neuropathology-predicted and actual cognitive changes (*$p < 0.05$, the *p* value from the one-sided regional-specificity control analysis is reported here instead of the correlation test *p* value). No multiple-comparison correction was applied. ADNI global cognition includes memory, executive function, and language cognition scores. dMemory (delayed memory recall) score includes logical memory delayed recall (LMDR) and delayed word recall from the Alzheimer's Disease Assessment Scale–Cognitive Subscale (DWR-ADASc).

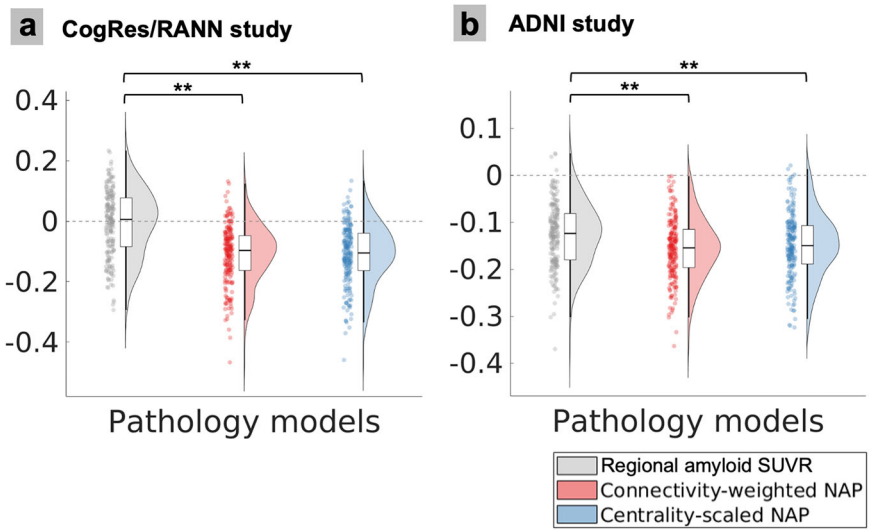

Fig. 6 | Correlation results in the relationship between pathology features in each region of interest (ROI) and longitudinal cognitive decline. a For participants in the CogRes/RANN study, we performed a Spearman partial correlation analysis between pathology features in each ROI and longitudinal cognitive changes, controlling for age, sex, education, baseline cognition, and mean cortical thickness of each hemisphere. Pathology features were characterized by either regional standardized uptake value ratio (SUVR) or network-based amyloid-β pathology (NAP). **b** Same approach was performed for participants in the ADNI study. Compared to regional SUVR measures, NAP scores demonstrated a significantly stronger negative relationship with cognition change in both studies (In the CogRes/RANN study: connectivity-weighted NAP: $p < 6.06e\text{-}21$; centrality-scaled NAP: $p < 1.19e\text{-}20$; In the ADNI study: connectivity-weighted NAP: $p < 1.01e\text{-}05$; centrality-scaled NAP: $p < 1.30e\text{-}03$). Cognition was assessed using global cognition in the CogRes/RANN study and dMemory in the ADNI study. The analysis included seventy-seven participants in the CogRes/RANN study and seventy-two participants in the ADNI study. (**$p < 0.01$; two-sample Student's *t*-test).

cognition score (ADNI-GCog; summarized score of memory, executive functioning, and language)[45]; (3) Delayed recall tests of memory (dMemory; summarized score of logical memory delayed total recall and delayed word recall). The longitudinal change in the ADNI cognition scores is illustrated in Fig. S5.

To test the generalizability of the Aβ neuropathological signature, PET and MRI imaging data from the ADNI were preprocessed, and structural connectome and pathological measures were computed in the same way as the CogRes/RANN dataset. The sum of pathology features in the signature pattern was used to predict cognitive decline in ADNI cognition scores (residual score controlling for covariates). The predicted scores significantly correlated with the actual cognitive decline scores in dMemory (regional SUVR: $R = 0.2583$, $p < 0.0285$; connectivity-weighted NAP: $R = 0.3121$, $p < 0.0076$; centrality-scaled NAP: $R = 0.3018$, $p < 0.0100$; Fig. 5), but not in ADNI-GCog (regional SUVR: $R = 0.1894$, $p > 0.1136$; connectivity-weighted NAP: $R = 0.1902$, $p > 0.1121$; centrality-scaled NAP: $R = 0.1858$, $p > 0.1209$) and ADNI-Mem (regional SUVR: $R = 0.1456$, $p > 0.2257$; connectivity-weighted NAP: $R = 0.1264$, $p > 0.2937$; centrality-scaled NAP: $R = 0.1188$, $p > 0.3237$).

Besides predictive performance on cognitive decline, we additionally tested if the observed relationship is specific to these particular sets of regions in the amyloid-β neuropathological signature, i.e., regional specificity. To do this, we performed a control analysis involving random selection of a set of ROIs, ensuring that the number of ROIs matched those selected in the Aβ neuropathological signature. Then, features in this random ROI set were used to predict cognitive decline, and the correlation coefficient with the actual cognitive decline score was recorded. By repeating this random selection process 500 times, we generated a distribution of correlation values from these random ROI selections. As shown in Table 2, the results demonstrated that the regional SUVR of Aβ neuropathological signature significantly outperformed the randomly selected ROIs in predicting ADNI-GCog ($p < 0.0379$) and dMemory ($p < 0.0140$; Fig. 5a), but not in ADNI-Mem ($p > 0.1836$). And the connectivity-weighted NAP measures of Aβ neuropathological signature significantly outperformed the randomly selected ROIs in predicting dMemory ($p < 0.0120$; Fig. 5b), but not in predicting ADNI-Mem ($p > 0.0978$) and ADNI-GCog ($p > 0.4271$). The centrality-scaled NAP measures did not show significant regional specificity in any of the cognition tests (dMemory: $p > 0.0838$; ADNI-Mem: $p > 0.1497$; ADNI-GCog: $p > 0.6467$; Fig. 5c). Together, the results demonstrated that the Aβ neuropathological signature generalizes to an external dataset for predicting cognitive decline, and patterns derived from regional SUVR and connectivity-weighted NAP demonstrate regional specificity.

Lastly, we evaluated whether the proposed NAP scores are more sensitive to cognitive decline than regional SUVR scores when not using a cross-validation model, which may perform better due to optimized data-driven feature selection. We performed a Spearman partial correlation analysis between pathology features in each ROI and longitudinal cognitive changes, controlling for age, sex, education, baseline cognition, and mean cortical thickness of each hemisphere. As shown in Fig. 6, using a two-sample Student's *t*-test, both NAP scores exhibited a significantly stronger

negative correlation with cognitive changes compared to regional SUVR scores in both the CogRes/RANN (Connectivity-weighted NAP: $t = 9.9404$, $p < 6.0630e\text{-}21$; centrality-scaled NAP: $t = 9.8563$, $p < 1.1907e\text{-}20$) and ADNI datasets (Connectivity-weighted NAP: $t = 4.4735$, $p < 1.0054e\text{-}5$; centrality-scaled NAP: $t = 3.2465$, $p < 0.0013$), where cognition was assessed using global cognition and dMemory, respectively. Network-level correlation results, based on networks defined by the Schaefer atlas, are provided in Fig. S6. In addition to regional specificity, the results demonstrated higher sensitivity of the proposed NAP scores to cognitive decline compared to regional SUVR scores.

The observed relationships between NAP measures and longitudinal cognitive decline cannot be fully explained by tau pathology

Given that tau PET measures are strongly associated with cognitive decline[70,75,76], we additionally tested whether the observed relationships between cognition and amyloid could be explained by tau pathology. We used both global and temporal lobe tau PET SUVR values from follow-up visits to quantify tau pathology, and the analysis was performed on a subset of participants with available tau PET data ($N = 27$). While our results showed that longitudinal cognitive decline was significantly associated with global connectivity-weighted NAP measures ($r = -0.5543$, $p = 0.0091$; Spearman correlation controlling for age, sex, education, and baseline cognition), this relationship remained significant after adjusting for future global tau SUVR ($r = -0.4673$, $p = 0.0378$) and for temporal lobe tau SUVR ($r = -0.4892$, $p = 0.0286$) as covariates. However, longitudinal cognitive decline was not significantly associated with global amyloid SUVR, either before ($r = -0.3273$, $p = 0.1476$) or after adjusting for tau pathology (controlling for global tau: $r = -0.2261$, $p = 0.3377$; controlling for temporal lobe tau: $r = -0.2243$, $p = 0.3418$). We then repeated these analyses for the relationships between longitudinal cognitive decline and amyloid measures in the identified neuropathological signature regions. The relationships were significant for regional amyloid SUVR in the signature regions (Fig. 5a), both before ($r = -0.4622$, $p = 0.0349$) and after adjusting for tau pathology (controlling for global tau: $r = -0.5297$, $p = 0.0163$; controlling for temporal lobe tau: $r = -0.5039$, $p = 0.0235$). Similarly, the associations remained significant for connectivity-weighted NAP measures in the signature regions (Fig. 5b), both before ($r = -0.6284$, $p = 0.0023$) and after including tau pathology as a covariate (controlling for global tau: $r = -0.5746$, $p = 0.0081$; controlling for temporal lobe tau: $r = -0.5979$, $p = 0.0054$). These analyses indicate that the observed associations between amyloid-related measures and longitudinal cognitive decline cannot be fully explained by tau burden. Nevertheless, given the central role of tau in neurodegeneration and cognitive decline, further investigation with larger samples of tau PET data is warranted.

Discussion

Aβ deposition in the brain is an important hallmark of AD, sometimes occurring decades before the onset of cognitive impairment. However, the relationship between early deposition of Aβ and future cognitive decline is still unclear, especially since we did not have an effective metric of brain Aβ that is predictive of future cognition. Here, we established a cross-validated predictive model to examine our proposed network-based Aβ pathology measures. A comprehensive examination evaluated predictive validity and external generalization. There were several important findings. First, early Aβ regional pathology significantly predicted future cognitive decline in global cognition. Second, incorporating structural connectome, but not functional connectome, information into pathology measures improved predictive performance. Lastly, the Aβ neuropathological signatures derived from our internal dataset generalize to external dataset validation.

Current correlation-based approaches for studying the amyloid-cognition relationship often fall short in providing informative insights for future studies, primarily due to the nature of their within-sample validation, which limits the generalizability of findings. In this study, we adapted a cross-validated predictive modeling approach, based on the CPM framework, to test the predictive validity of early Aβ deposition measures on future cognitive decline, where the performance was validated in held-out samples during cross-validation. Cross-validated predictive models, such as CPM, have been widely used to investigate brain-behavior relationships across various domains. For example, such models have been employed to study the relationship between resting-state functional connectivity and attention[30], AD-related cognitive deficits[77], task-based functional connectivity and creative ability[78], cognitive reserve[79], aggressive behavior[80], as well as structural network lesioning with cognitive control[32] and stroke-related motor impairments[81]. However, such approaches have not been commonly used to study neuropathology and cognitive aging. In this study, we demonstrated, using the cross-validated predictive modeling, that early Aβ regional pathology significantly predicts future cognitive decline in global cognition. Although previous research has established associations between Aβ deposition and cognitive decline in specific domains such as processing speed[14], executive function[82], vocabulary and language[14,17], and visuospatial function[15,83], our study focused on global cognition because it is consistently reported to be associated with early Aβ deposition[14,15,83–85], and demonstrated a stronger effect size compared to cognitions in individual domains[15]. Consistent with the literature, we did not observe significant relationships when models were trained on cognitive decline within cognitive domains. The stronger effect of Aβ on global cognition may reflect the downstream impact of Aβ on subsequent neuropathological processes, potentially contributing to a more pronounced relationship with clinical outcomes over time[18]. Our findings contribute to understanding regionally specific deposition of Aβ and its contributions to future cognitive decline.

It is well-established that early Aβ deposition exhibits a significant yet weak relationship with future cognitive decline. Given the multifaceted nature of AD, it is crucial to revisit the amyloid-cognition relationship by considering more comprehensive factors. Current studies often overlook the potential contribution of network-level metrics of neuropathology to subsequent cognitive decline. However, network-based approaches are important because neurological symptoms are increasingly understood to correlate more closely with dysfunction in brain networks rather than with deficits in specific locations. For instance, the lesion-network mapping approach[86] leverages the brain connectome to map common networks underlying lesions in different locations that manifest similar clinical symptoms. This method has been successfully applied to neuropsychiatric conditions such as amnesia[87], depression[88], and addiction remission[89]. Despite these advances, the network mapping of neuropathology in AD remains largely unexplored. Moreover, emerging evidence suggests that the spread of molecular neuropathology, as well as neurodegenerative damage, may follow large-scale brain networks[20,90]. It is important to consider the spatial patterns of neuropathology deposition. Growing evidence shows that neuropathology distribution exhibits spatial heterogeneity and subtype structures. This was first observed in tau pathology[91] and more recently in Aβ deposition, where distinct subtypes have been identified, such as frontal, parietal, and occipital predominant subtypes[29] as well as temporal and cingulate predominant subtypes[24]. To relate network-based pathology and cognition, Luan et al. employed a lesion-network mapping approach to tau pathology, identifying distinct tau-lesion-network maps associated with cognitive deficits in different cognitive domains[21]. Building upon such concepts, our study introduces NAP quantifications of Aβ deposition, utilizing subject-specific connectivity profiles (either structural or functional) to map networks associated with local Aβ deposition. Our approach is conceptually aligned with lesion-network mapping[86] and white-matter disconnection scores[32,81], but we propose a more continuous and personalized metric that incorporates current understanding of the neuropathology underlying AD. For example, in our connectivity-weighted NAP measures, we use personalized connection strength as weights, reflecting the notion that stronger connections may facilitate faster pathology spread[20]. Additionally, our centrality-scaled measure is based on the idea that the pathology deposition in highly connected brain regions (regions of high topological centrality) may lead to more severe cognitive decline due to their widespread effects on brain dynamics[72]. It was also built upon the

observations in the literature that Aβ pathology preferentially affects high centrality hub regions, demonstrating selective vulnerability in hub regions[92]. Centrality-based pathology measures, such as the tau hub ratio[93], have been proposed to assess tau pathology and have been associated with cognitive decline. Our proposed centrality-scaled NAP measure builds on this prior work by utilizing subject-specific connectomes, offering a more individualized approach compared to group-average connectome methods. Our study provides the first characterization of network-level Aβ pathology and demonstrates that incorporating network connectome information into pathology measures enhances the predictive performance for subsequent cognitive decline compared to regional measures.

Our NAP approach does not assume premorbid or healthy connectivity. Instead, we use each individual's baseline connectome, regardless of whether it reflects normal variation or disease effects, as a framework to summarize baseline regional amyloid burden. This allows us to examine how amyloid is distributed within the individual's brain network architecture at baseline. While some confounding factors, such as biological variability and disease-related alterations, may exist, our experiments show that individualized NAP measures better predict cognitive decline than template-based or connectome-only models (see Supplementary Materials for details). Our results highlighted the important role of the individual connectome between neuropathology and cognition, which is important for early detection of AD-related cognitive deficits at the individual level. However, it remains unclear which attributes of the interplay between brain network architecture and neuropathology are responsible for the increased predictive performance. There are several potential candidate mechanisms: (1) Individual connectomes capture coordinated regions that are selectively vulnerable to Aβ pathology. It has been shown that specific neurons, brain regions, and brain networks exhibit selective vulnerability to neuropathology[8,94–97]. Highly connected hub regions with higher levels of neuronal activity and metabolic demand are vulnerable to neuropathology[92,98,99]. The proposed centrality-scaled NAP score, considering nodal centrality, may reflect networks with vulnerable hubs for the given subject, where severe AD-related symptoms might develop if Aβ disrupts highly functioning vulnerable hubs. (2) Individual connectomes are indicative of future Aβ spread and accumulation. Recent evidence suggested that many neurodegenerative disease-related pathological proteins (e.g., Aβ, tau, and α-synuclein) exhibit intercellular transmission[100]. This suggests that the early deposition of Aβ can potentially spread trans-neuronally across large-scale brain networks[98,101–103]. Thus, the selective vulnerability might be a result of the spreading between anatomically connected brain regions[100]. For example, Song et al.[101] provided both in vitro and in vivo evidence supporting the transmission of Aβ via neuronal connections[101]. The predictive utility of the NAP measure may therefore reflect connectivity-mediated propagation of Aβ pathology or the spread of Aβ-associated hyperactivity[104]. However, it is also possible that the NAP captures regions of amyloid and tau co-localization, particularly given the stronger evidence for network-based spread of tau and its closer association with cognitive decline. Future longitudinal studies combining Aβ and tau PET, along with structural connectivity, will be essential to further elucidate the biological mechanisms underlying these network-level neuroimaging biomarkers. Some studies have shown that neuropathology progression along the structural connectome can be modeled to predict its future regional deposition[105]. The proposed connectivity-weighted NAP score, considering nodal connectivity profile (either structural or functional), may suggest future Aβ spread based on its baseline deposition, where future deposition more closely tracks cognitive decline in the future. (3) Individual connectomes reflect the resilience of brain networks to neuropathology. Recent studies have found that topological characteristics of brain network resilience are related to age and cognition[106]. Incorporating connectome information into the pathology measures might account for individual resilience factors, and explain more variance in the cognition[18,107,108].

Incorporating structural connectome into NAP measures significantly improves the prediction of future cognitive decline; however, this is not the case for functional connectome-based NAP measures. One explanation for this is that functional connectivity reflects not only direct monosynaptic connections but also indirect polysynaptic connections[109]. Because functional connectivity quantifies statistical dependency between regional neural signals, the observed interactions between two regions might be mediated by other regions[110]. Trans-synaptic propagation of misfolded proteins might be shaped more by the structural than functional connections. Another possible explanation is that the complex interplay between Aβ deposition and brain fMRI signals is often reported and not well understood. Some studies suggest that Aβ deposition leads to increased neural activity, and this hyperactivity may eventually lead to more rapid secretion of amyloid, forming a vicious cycle of Aβ accumulation and abnormal brain function[111]. The proposed simple NAP approach is not well-suited to capture such complex interplay between fMRI signal and neuropathology. The present work may inform future studies on the complex interplay between brain network architecture, neuropathology, and cognition.

The neuropathological signature patterns identified in our study encompass regions within the default mode, cognitive control, visual, limbic, and salience networks, including the visual areas, temporal-occipital junction, temporal pole, insula, medial prefrontal cortex, lateral prefrontal cortex, orbitofrontal cortex, and parahippocampus. These regions are consistent with previous findings on early-stage Aβ deposition, where the initial deposition was observed in the basal portions of the frontal, temporal, and occipital lobes[26,112]. While studies reported early Aβ presence in basal visual areas[26,113], other studies suggested amyloid reaches the visual cortex at later stages[7,74]. This inconsistency might be explained by recent work that identified an occipital subtype of Aβ accumulation, characterized by early abnormalities in the occipital cortex and a higher number of participants with dementia in such a subtype compared to other subtypes[29]. Aβ deposition in the occipital cortex was often overlooked, whereas its deposition within the occipital cortex has already been associated with cerebral amyloid angiopathy[114] and Lewy body disease[115]. Recent studies also demonstrated neurophysiological measures during a visual processing task that are sensitive to amyloid pathology in early-stage AD[116]. Our findings further support the notion that early Aβ deposition in the occipital lobe provides prognostic information for future cognitive decline. However, more studies are needed to investigate the relationship between Aβ occipital deposition and cognition. Moreover, the Aβ neuropathological signature derived from our internal dataset serves as a generalizable predictor of cognitive decline in the external dataset, demonstrating a consistent relationship with cognition across datasets as well as consistent regional specificity. However, the predictive power of our model is somewhat attenuated in the ADNI dataset, likely due to variations in PET radiotracers and diffusion MRI acquisition parameters that impact the structural connectome[117].

The cross-validated predictive framework used here can be extended to other neuropathological and neurodegenerative markers, such as tau, α-synuclein, cortical atrophy, longitudinal Aβ accumulation[118], or a composite measure of ATN (amyloid, tau, neurodegeneration) features[69]. Corresponding NAP scores for each measure can be computed to quantify its network-level effects and test their predictive performance on cognition. Additionally, future research should explore how cognitive reserve and resilience factors might moderate the relationship between Aβ accumulation and cognitive decline[18,108]. For example, increased brain activity and connectivity have often been observed alongside Aβ deposition[8], potentially promoting cognitive reserve and helping to maintain cognitive function[119]. The high prediction performance of the proposed NAP might be attributed to its indication of future network propagation or network disruption of the vulnerable region due to initial Aβ deposition and individualized connectome. This framework demonstrated superior predictive performance for future cognitive decline compared to regional Aβ pathology alone. However, these hypotheses on the underlying mechanisms need to be tested in future studies.

The current study has several limitations. First, the sample size in this study is small, particularly considering that cognitive decline in cognitively normal older adults is expected to be mild. The proposed framework needs

to be validated with larger sample sizes to further ensure its robustness and generalizability. Second, since Aβ deposition is considered an early event in the neuropathological cascade of AD, we focused on the predictive validity of baseline Aβ deposition for future cognitive decline. However, the impact of Aβ on cognition is more complex, involving interactions with multiple factors that jointly affect cognitive outcomes. Specifically, in this study, we did not account for tau deposition or genomic information, such as APOE ε4 status, which may mediate the observed effects of Aβ on cognition. For example, evidence showed that high Aβ levels are associated with tau accumulation in the medial temporal lobe[4], and Aβ and tau have interactive effects on cognitive decline[120]. Additionally, Aβ interacts with APOE ε4 to promote cognitive decline in cognitively normal older adults[121], but APOE ε4 status was not included in our analysis. Aβ also interacts closely with neurodegenerative factors, such as hippocampal volume, glucose metabolism[122], and cortical atrophy[123]. While we included hemispheric mean cortical thickness as a confounder, future studies should examine regional atrophy and its role in the Aβ-cognition relationship. Regional atrophy was not included in this study due to limitations in sample size. Finally, future studies with longitudinal assessment of Aβ accumulation rates could provide additional insights into Aβ pathology[118]; however, recent evidence suggests that longitudinal measures may not significantly enhance the detection of cognitive decline compared to a single Aβ PET scan session[85]. In general, future research should comprehensively evaluate the potential factors that interact with Aβ pathology to better understand its relationship with future cognitive decline. Such a multimodal approach would be well-suited to capture the multifaceted nature of AD. Here, the proposed network-based approach and predictive modeling framework can be easily adapted to include other neuropathologies. And it would be intriguing to investigate an optimal combination of AD-related features, such as a composite score from ATN measures. These could be used to build and validate network-based predictive models for AD-related symptoms, similar to the framework proposed in this study, thereby promoting early detection of individuals on the AD continuum.

Furthermore, in this study, we focused on cognitive decline in cognitively normal older adults, which captures early and subtle changes that do not meet clinical thresholds. Studying this population minimizes the influence of confounding factors such as co-pathologies and clinical heterogeneity present in symptomatic individuals. This allows a clearer assessment of early amyloid-related indicators of neurodegenerative processes. Nonetheless, it is important to test and extend this framework to participants across the full AD spectrum in future research. Although in our sample, we did not identify any amyloid-related pathology measures that were associated with preserved or improved cognitive performance, this remains an important topic for future research to investigate whether specific network features are linked to cognitive resilience or compensatory mechanisms.

In summary, we developed a cross-validated predictive model to assess Aβ pathology measures for predicting future cognitive decline in cognitively normal older adults. Our results demonstrated that early regional Aβ pathology is a significant predictor of global cognitive decline, with predictive accuracy further enhanced by incorporating individualized structural connectome data as network-based Aβ pathology scores. The identified neuropathological signature pattern is indicative of future cognitive decline and demonstrates generalizability to external datasets. This network-based approach and predictive modeling complement existing pathology-based methods for early detection of individuals at risk of developing AD-related symptoms and can be extended to other neuropathological markers. The framework supports future neurodegenerative disease research that considers individual brain network connectivity when evaluating neuropathology and cognition.

Data availability

The numerical results underlying the figures are provided in the Supplementary Data: Fig. 3—Supplementary Data 1; Fig. 4—Supplementary Data 2; Fig. 5—Supplementary Data 3; Fig. 6—Supplementary Data 4. Name, labels, and centroid coordinates of the brain regions in the neuropathological signatures are provided in the Supplementary Data 5. Demographic information, processed PET SUVR, and brain connectivity data are available at https://doi.org/10.6084/m9.figshare.30152470.v1[124] and https://github.com/hehengda/cross_validation_network_based_amyloid.git. The raw and preprocessed CogRes/RANN datasets analyzed in the current study are available from the corresponding author on reasonable request. ADNI data can be accessed through the ADNI database (adni.loni.usc.edu) following registration and compliance with the data usage agreement.

Code availability

The code used in this project and sample data are available at https://doi.org/10.6084/m9.figshare.30152470.v1[124] and https://github.com/hehengda/cross_validation_network_based_amyloid.git.

Received: 1 February 2025; Accepted: 29 September 2025;
Published online: 05 December 2025

References

1. Hardy, J. A. & Higgins, G. A. Alzheimer's disease: the amyloid cascade hypothesis. *Science* **256**, 184–185 (1992).
2. Karran, E., Mercken, M. & Strooper, B. De. The amyloid cascade hypothesis for Alzheimer's disease: an appraisal for the development of therapeutics. *Nat. Rev. Drug Discov.* **10**, 698–712 (2011).
3. Pooler, A. M. et al. Amyloid accelerates tau propagation and toxicity in a model of early Alzheimer's disease. *Acta Neuropathol. Commun.* **3**, 14 (2015).
4. Wha Jin Lee, A. et al. In brief Regional Ab-tau interactions promote onset and acceleration of Alzheimer's disease tau spreading. *Neuron* **110**, 1932–1943.e5 (2022).
5. Leng, F. & Edison, P. Neuroinflammation and microglial activation in Alzheimer disease: where do we go from here? *Nat. Rev. Neurol.* **17**, 157–172 (2020).
6. Doré, V. et al. Cross-sectional and longitudinal analysis of the relationship between Aβ deposition, cortical thickness, and memory in cognitively unimpaired individuals and in Alzheimer disease. *JAMA Neurol.* **70**, 903–911 (2013).
7. Palmqvist, S. et al. Earliest accumulation of β-amyloid occurs within the default-mode network and concurrently affects brain connectivity. *Nat. Commun.* **8**, 1–13 (2017).
8. Sperling, R. A. et al. Amyloid Deposition Is Associated with Impaired Default Network Function in Older Persons without Dementia. *Neuron* **63**, 178–188 (2009).
9. Hampel, H. et al. The Amyloid-β Pathway in Alzheimer's Disease. *Mol. Psychiatry* **26**, 5481–5503 (2021).
10. Aizenstein, H. J. et al. Frequent amyloid deposition without significant cognitive impairment among the elderly. *Arch. Neurol.* **65**, 1509–1517 (2008).
11. Sperling, R. A. et al. Toward defining the preclinical stages of Alzheimer's disease: recommendations from the National Institute on Aging-Alzheimer's Association workgroups on diagnostic guidelines for Alzheimer's disease. *Alzheimers Dement.* **7**, 280 (2011).
12. Rowe, C. C. et al. Amyloid imaging results from the Australian Imaging, Biomarkers and Lifestyle (AIBL) study of aging. *Neurobiol. Aging* **31**, 1275–1283 (2010).
13. Lim, Y. Y. et al. Effect of amyloid on memory and non-memory decline from preclinical to clinical Alzheimer's disease. *Brain* **137**, 221–231 (2014).
14. Farrell, M. E. et al. Association of longitudinal cognitive decline with amyloid burden in middle-aged and older adults: evidence for a dose-response relationship. *JAMA Neurol.* **74**, 830–838 (2017).
15. Baker, J. E. et al. Cognitive impairment and decline in cognitively normal older adults with high amyloid-β: a meta-analysis. *Alzheimer's. Dement.* **6**, 108–121 (2017).

16. Harrington, K. D. et al. Amyloid β-associated cognitive decline in the absence of clinical disease progression and systemic illness. *Alzheimer's. Dement.* **8**, 156 (2017).
17. Lao, P. J. et al. Amyloid, cerebrovascular disease, and neurodegeneration biomarkers are associated with cognitive trajectories in a racially and ethnically diverse, community-based sample. *Neurobiol. Aging* **117**, 83–96 (2022).
18. Jagust, W. J., Teunissen, C. E. & DeCarli, C. The complex pathway between amyloid β and cognition: implications for therapy. *Lancet Neurol.* **22**, 847–857 (2023).
19. Vogel, J. W. et al. Spread of pathological tau proteins through communicating neurons in human Alzheimer's disease. *Nat. Commun.* **11**, 1–15 (2020).
20. Vogel, J. W. et al. Connectome-based modelling of neurodegenerative diseases: towards precision medicine and mechanistic insight. *Nat. Rev. Neurosci.* **24**, 620–639 (2023).
21. Luan, Y., Franzmeier, N., Rubinski, A. & Ewers, M. Lesion-network mapping of tau accumulation is predictive of domain-specific cognitive deficits in Alzheimer's disease. *Alzheimer's. Dement.* **17**, e050775 (2021).
22. Farrell, M. E. et al. Spatial extent as a sensitive amyloid-PET metric in preclinical Alzheimer's disease. *Alzheimers Dement.* https://doi.org/10.1002/ALZ.14036 (2024).
23. Farrell, M. E. et al. Regional amyloid accumulation and cognitive decline in initially amyloid-negative adults. *Neurology* **91**, E1809–E1821 (2018).
24. Alchera, N. et al. Patterns of amyloid accumulation in amyloid-negative cases. *Neurobiol. Aging* **129**, 99–108 (2023).
25. Buckner, R. L. et al. Cortical hubs revealed by intrinsic functional connectivity: mapping, assessment of stability, and relation to Alzheimer's disease. *J. Neurosci.* **29**, 1860–1873 (2009).
26. Braak, H. & Braak, E. Neuropathological stageing of Alzheimer-related changes. *Acta Neuropathol.* **82**, 239–259 (1991).
27. Thal, D. R., Rüb, U., Orantes, M. & Braak, H. Phases of Aβ-deposition in the human brain and its relevance for the development of AD. *Neurology* **58**, 1791–1800 (2002).
28. Fantoni, E., Collij, L., Alves, I. L., Buckley, C. & Farrar, G. The spatial-temporal ordering of amyloid pathology and opportunities for PET imaging. *J. Nucl. Med.* **61**, 166–171 (2020).
29. Collij, L. E. et al. Spatial-temporal patterns of β-amyloid accumulation: a subtype and stage inference model analysis. *Neurology* **98**, E1692–E1703 (2022).
30. Rosenberg, M. D. et al. A neuromarker of sustained attention from whole-brain functional connectivity. *Nat. Neurosci.* **19**, 165–171 (2015).
31. Shen, X. et al. Using connectome-based predictive modeling to predict individual behavior from brain connectivity. *Nat. Protoc.* **12**, 506–518 (2017).
32. Jiang, J., Bruss, J., Lee, W. T., Tranel, D. & Boes, A. D. White matter disconnection of left multiple demand network is associated with post-lesion deficits in cognitive control. *Nat. Commun.* **14**, 1–12 (2023).
33. Stern, Y. Cognitive reserve in ageing and Alzheimer's disease. *Lancet Neurol.* **11**, 1006–1012 (2012).
34. Mattis, S. *Dementia Rating Scale (DRS): Professional Manual* (Psychological Assessment Resources, 1988).
35. Hani Hojjati, S., Feiz, F., Ozoria, S., Razlighi, Q. R. & Alzheimer's Disease Neuroimaging Initiative. Topographical overlapping of the amyloid-β and tau pathologies in the default mode network predicts Alzheimer's disease with higher specificity. *J. Alzheimers Dis.* **83**, 407–421 (2021).
36. Buschke, H. & Fuld, P. A. Evaluating storage, retention, and retrieval in disordered memory and learning. *Neurology* **24**, 1019–1025 (1974).
37. Wechsler, D. *Wechsler Adult Intelligence Scale* (Harcourt Assessment, 1997).
38. Holdnack, H. A. *Wechsler Test of Adult Reading: WTAR* (The Psychological Corporation, 2001).
39. Golden, C. J. A group version of the Stroop Color and Word Test. *J. Pers. Assess.* **39**, 386–388 (1975).
40. Reitan, R. M. *Manual for Administration of Neuropsychological Test Batteries for Adults and Children* (Psychological Corporation, 1978).
41. Crane, P. K. et al. Development and assessment of a composite score for memory in the Alzheimer's Disease Neuroimaging Initiative (ADNI). *Brain Imaging Behav.* **6**, 502–516 (2012).
42. Mohs, R. C. et al. Development of cognitive instruments for use in clinical trials of antidementia drugs: additions to the Alzheimer's Disease Assessment Scale that broaden its scope. *Alzheimer Dis. Assoc. Disord.* **11**, 13–21 (1997).
43. Gibbons, L. E. et al. A composite score for executive functioning, validated in Alzheimer's Disease Neuroimaging Initiative (ADNI) participants with baseline mild cognitive impairment. *Brain Imaging Behav.* **6**, 517 (2012).
44. Nasreddine, Z. S. et al. The Montreal Cognitive Assessment, MoCA: A Brief Screening Tool For Mild Cognitive Impairment. *J. Am. Geriatr. Soc.* **53**, 695–699 (2005).
45. Choi, S. E. et al. Development and validation of language and visuospatial composite scores in ADNI. *Alzheimer's. Dement.* **6**, e12072 (2020).
46. Fischl, B. et al. Automatically parcellating the human cerebral cortex. *Cereb. Cortex* **14**, 11–22 (2004).
47. Desikan, R. S. et al. An automated labeling system for subdividing the human cerebral cortex on MRI scans into gyral based regions of interest. *Neuroimage* **31**, 968–980 (2006).
48. Schaefer, A. et al. Local-global parcellation of the human cerebral cortex from intrinsic functional connectivity MRI. *Cereb. Cortex* **28**, 3095–3114 (2018).
49. Fischl, B. et al. Whole Brain segmentation: automated labeling of neuroanatomical structures in the human brain. *Neuron* **33**, 341–355 (2002).
50. Fjell, A. M. et al. High consistency of regional cortical thinning in aging across multiple samples. *Cereb. Cortex* **19**, 2001–2012 (2009).
51. Tahmi, M., Bou-Zeid, W. & Razlighi, Q. R. A fully automatic technique for precise localization and quantification of amyloid-β PET scans. *J. Nucl. Med.* **60**, 1771 (2019).
52. Razlighi, Q. R. et al. Unilateral disruptions in the default network with aging in native space. *Brain Behav.* **4**, 143–157 (2014).
53. Smith, S. M. et al. Advances in functional and structural MR image analysis and implementation as FSL. *Neuroimage* **23**, S208–S219 (2004).
54. Jenkinson, M., Bannister, P., Brady, M. & Smith, S. Improved optimization for the robust and accurate linear registration and motion correction of brain images. *Neuroimage* **17**, 825–841 (2002).
55. Power, J. D., Barnes, K. A., Snyder, A. Z., Schlaggar, B. L. & Petersen, S. E. Spurious but systematic correlations in functional connectivity MRI networks arise from subject motion. *Neuroimage* **59**, 2142–2154 (2012).
56. Mansour L, S. et al. Connectomes for 40,000 UK Biobank participants: A multi-modal, multi-scale brain network resource. *Neuroimage* **283**, 120407 (2023).
57. Tahedl, M. B.A.T.M.A.N.: Basic and Advanced Tractography with MRtrix for All Neurophiles. https://doi.org/10.17605/OSF.IO/FKYHT (2017).
58. Tournier, J. D. et al. MRtrix3: a fast, flexible and open software framework for medical image processing and visualisation. *Neuroimage* **202**, 116137 (2019).
59. Veraart, J. et al. Denoising of diffusion MRI using random matrix theory. *Neuroimage* **142**, 394–406 (2016).

60. Kellner, E., Dhital, B., Kiselev, V. G. & Reisert, M. Gibbs-ringing artifact removal based on local subvoxel-shifts. *Magn. Reson. Med.* **76**, 1574–1581 (2016).
61. Andersson, J. L. R., Skare, S. & Ashburner, J. How to correct susceptibility distortions in spin-echo echo-planar images: application to diffusion tensor imaging. *Neuroimage* **20**, 870–888 (2003).
62. Andersson, J. L. R. & Sotiropoulos, S. N. An integrated approach to correction for off-resonance effects and subject movement in diffusion MR imaging. *Neuroimage* **125**, 1063–1078 (2016).
63. Tustison, N. J. et al. N4ITK: improved N3 bias correction. *IEEE Trans. Med. Imaging* **29**, 1310–1320 (2010).
64. Poldrack, R. A., Huckins, G. & Varoquaux, G. Establishment of best practices for evidence for prediction: a review. *JAMA Psychiatry* **77**, 534–540 (2020).
65. Varoquaux, G. et al. Assessing and tuning brain decoders: cross-validation, caveats, and guidelines. *Neuroimage* **145**, 166–179 (2017).
66. Luchsinger, J. A. et al. Pre-diabetes, but not type 2 diabetes, is related to brain amyloid in late middle-age. *J. Alzheimers Dis.* **75**, 1273–1282 (2020).
67. Villemagne, V. L. et al. Comparison of 11C-PiB and 18F-florbetaben for Aβ imaging in ageing and Alzheimer's disease. *Eur. J. Nucl. Med. Mol. Imaging* **39**, 983–989 (2012).
68. Sabri, O. et al. Florbetaben PET imaging to detect amyloid beta plaques in Alzheimer's disease: phase 3 study. *Alzheimers Dement.* **11**, 964–974 (2015).
69. Jack, C. R. et al. NIA-AA Research Framework: toward a biological definition of Alzheimer's disease. *Alzheimers Dement.* **14**, 535–562 (2018).
70. Aschenbrenner, A. J., Gordon, B. A., Benzinger, T. L. S., Morris, J. C. & Hassenstab, J. J. Influence of tau PET, amyloid PET, and hippocampal volume on cognition in Alzheimer disease. *Neurology* **91**, e859–e866 (2018).
71. Gabrieli, J. D. E., Ghosh, S. S. & Whitfield-Gabrieli, S. Prediction as a humanitarian and pragmatic contribution from human cognitive neuroscience. *Neuron* **85**, 11–26 (2015).
72. Fornito, A., Zalesky, A. & Breakspear, M. The connectomics of brain disorders. *Nat. Rev. Neurosci.* **16**, 159–172 (2015).
73. Garrison, K. A., Scheinost, D., Finn, E. S., Shen, X. & Constable, R. T. The (in)stability of functional brain network measures across thresholds. *Neuroimage* **118**, 651 (2015).
74. Grothe, M. J. et al. In vivo staging of regional amyloid deposition. *Neurology* **89**, 2031–2038 (2017).
75. Maass, A. et al. Alzheimer's pathology targets distinct memory networks in the ageing brain. *Brain* **142**, 2492–2509 (2019).
76. Ziontz, J. et al. Tau pathology in cognitively normal older adults. *Alzheimers Dement.* **11**, 637–645 (2019).
77. Svaldi, D. O. et al. Optimizing differential identifiability improves connectome predictive modeling of cognitive deficits from functional connectivity in Alzheimer's disease. *Hum. Brain Mapp.* **42**, 3500–3516 (2021).
78. Beaty, R. E. et al. Robust prediction of individual creative ability from brain functional connectivity. *Proc. Natl. Acad. Sci. USA* **115**, 1087–1092 (2018).
79. Boyle, R. et al. Connectome-based predictive modelling of cognitive reserve using task-based functional connectivity. *Eur. J. Neurosci.* **57**, 490–510 (2023).
80. Ibrahim, K. et al. Large-scale functional brain networks of maladaptive childhood aggression identified by connectome-based predictive modeling. *Mol. Psychiatry* **27**, 985–999 (2021).
81. Olafson, E. R. et al. Data-driven biomarkers better associate with stroke motor outcomes than theory-based biomarkers. *Brain Commun.* https://doi.org/10.1093/BRAINCOMMS/FCAE254 (2024).
82. Mielke, M. M. et al. Influence of amyloid and APOE on cognitive performance in a late middle-aged cohort. *Alzheimers Dement.* **12**, 281 (2016).
83. Petersen, R. C. et al. Association of elevated amyloid levels with cognition and biomarkers in cognitively normal people from the community. *JAMA Neurol.* **73**, 85–92 (2016).
84. Donohue, M. C. et al. Association between elevated brain amyloid and subsequent cognitive decline among cognitively normal persons. *JAMA* **317**, 2305–2316 (2017).
85. Chen, G. et al. Predicting cognitive decline: Which is more useful, baseline amyloid levels or longitudinal change? *Neuroimage Clin.* **41**, 103551 (2024).
86. Fox, M. D. Mapping symptoms to brain networks with the human connectome. *N. Engl. J. Med.* **379**, 2237–2245 (2018).
87. Ferguson, M. A. et al. A human memory circuit derived from brain lesions causing amnesia. *Nat. Commun.* **10**, 1–9 (2019).
88. Siddiqi, S. H. et al. Brain stimulation and brain lesions converge on common causal circuits in neuropsychiatric disease. *Nat. Hum. Behav.* **5**, 1707–1716 (2021).
89. Joutsa, J. et al. Brain lesions disrupting addiction map to a common human brain circuit. *Nat. Med.* **28**, 1249–1255 (2022).
90. Seeley, W. W., Crawford, R. K., Zhou, J., Miller, B. L. & Greicius, M. D. Neurodegenerative diseases target large-scale human brain networks. *Neuron* **62**, 42 (2009).
91. Vogel, J. W. et al. Four distinct trajectories of tau deposition identified in Alzheimer's disease. *Nat. Med.* **27**, 871–881 (2021).
92. Stam, C. J. Modern network science of neurological disorders. *Nat. Rev. Neurosci.* **15**, 683–695 (2014).
93. Frontzkowski, L. et al. Earlier Alzheimer's disease onset is associated with tau pathology in brain hub regions and facilitated tau spreading. *Nat. Commun.* **13**, 1–14 (2022).
94. Buckner, R. L. et al. Molecular, structural, and functional characterization of Alzheimer's disease: evidence for a relationship between default activity, amyloid, and memory. *J. Neurosci.* **25**, 7709–7717 (2005).
95. Pascoal, T. A. et al. Aβ-induced vulnerability propagates via the brain's default mode network. *Nat. Commun.* **10**, 1–13 (2019).
96. Surmeier, D. J., Obeso, J. A. & Halliday, G. M. Selective neuronal vulnerability in Parkinson disease. *Nat. Rev. Neurosci.* **18**, 101–113 (2017).
97. Fu, H., Hardy, J. & Duff, K. E. Selective vulnerability in neurodegenerative diseases. *Nat. Neurosci.* **21**, 1350 (2018).
98. Bero, A. W. et al. Neuronal activity regulates the regional vulnerability to amyloid-β deposition. *Nat. Neurosci.* **14**, 750–756 (2011).
99. Yu, M., Sporns, O. & Saykin, A. J. The human connectome in Alzheimer disease—relationship to biomarkers and genetics. *Nat. Rev. Neurol.* **17**, 545–563 (2021).
100. Peng, C., Trojanowski, J. Q. & Lee, V. M. Y. Protein transmission in neurodegenerative disease. *Nat. Rev. Neurol.* **16**, 199–212 (2020).
101. Song, H. L. et al. β-Amyloid is transmitted via neuronal connections along axonal membranes. *Ann. Neurol.* **75**, 88–97 (2014).
102. Goedert, M., Masuda-Suzukake, M. & Falcon, B. Like prions: the propagation of aggregated tau and α-synuclein in neurodegeneration. *Brain* **140**, 266–278 (2017).
103. Kim, H. R. et al. Comparison of amyloid β and tau spread models in Alzheimer's disease. *Cereb. Cortex* **29**, 4291 (2019).
104. Pignataro, A. & Middei, S. Trans-synaptic spread of amyloid-β in Alzheimer's disease: paths to β-amyloidosis. *Neural Plast.* **2017**, 5281829 (2017).
105. Yang, F. et al. Longitudinal predictive modeling of tau progression along the structural connectome. *Neuroimage* **237**, 118126 (2021).
106. Stanford, W. C., Mucha, P. J. & Dayan, E. A robust core architecture of functional brain networks supports topological resilience and cognitive performance in middle- and old-aged adults. *Proc. Natl. Acad. Sci. USA* **119**, e2203682119 (2022).

107. Rentz, D. M. et al. Cognition, reserve, and amyloid deposition in normal aging. *Ann. Neurol.* **67**, 353–364 (2010).
108. Stern, Y. et al. Whitepaper: Defining and investigating cognitive reserve, brain reserve, and brain maintenance. *Alzheimers Dement.* **16**, 1305–1311 (2020).
109. Grandjean, J., Zerbi, V., Balsters, J. H., Wenderoth, N. & Rudin, M. Structural basis of large-scale functional connectivity in the mouse. *J. Neurosci.* **37**, 8092–8101 (2017).
110. Reid, A. T. et al. Advancing functional connectivity research from association to causation. *Nat. Neurosci.* **22**, 1751–1760 (2019).
111. Leal, S. L., Landau, S. M., Bell, R. K. & Jagust, W. J. Hippocampal activation is associated with longitudinal amyloid accumulation and cognitive decline. *eLife* **6**, e22978 (2017).
112. Braak, H. & Braak, E. Frequency of stages of Alzheimer-related lesions in different age categories. *Neurobiol. Aging* **18**, 351–357 (1997).
113. Huang, K. L. et al. Regional amyloid deposition in amnestic mild cognitive impairment and Alzheimer's disease evaluated by [18F] AV-45 positron emission tomography in Chinese population. *PLoS ONE* **8**, e58974 (2013).
114. Johnson, K. A. et al. Imaging of amyloid burden and distribution in cerebral amyloid angiopathy. *Ann. Neurol.* **62**, 229–234 (2007).
115. Kantarci, K. et al. β-Amyloid PET and neuropathology in dementia with Lewy bodies. *Neurology* **94**, e282 (2020).
116. Javitt, D. C. et al. Disruption of early visual processing in amyloid-positive healthy individuals and mild cognitive impairment. *Alzheimers Res. Ther.* **15**, 1–12 (2023).
117. Sotiropoulos, S. N. & Zalesky, A. Building connectomes using diffusion MRI: Why, how and but. *NMR Biomed.* **32**, e3752 (2019).
118. Bischof, G. N. & Jacobs, H. I. L. Subthreshold amyloid and its biological and clinical meaning: long way ahead. *Neurology* **93**, 72–79 (2019).
119. Hahn, A. et al. Association between earliest amyloid uptake and functional connectivity in cognitively unimpaired elderly. *Cereb. Cortex* **29**, 2173–2182 (2019).
120. Sperling, R. A. et al. The impact of amyloid-beta and tau on prospective cognitive decline in older individuals. *Ann. Neurol.* **85**, 181–193 (2019).
121. Mormino, E. C. et al. Amyloid and APOE ε4 interact to influence short-term decline in preclinical Alzheimer disease. *Neurology* **82**, 1760 (2014).
122. Mormino, E. C. et al. Synergistic effect of β-amyloid and neurodegeneration on cognitive decline in clinically normal individuals. *JAMA Neurol.* **71**, 1379–1385 (2014).
123. Chételat, G. et al. Accelerated cortical atrophy in cognitively normal elderly with high β-amyloid deposition. *Neurology* **78**, 477–484 (2012).
124. He, H., Habeck, C. & Stern, Y. Custom code and data for 'Integrating individualized connectome with amyloid pathology improves predictive modeling of future cognitive decline'. https://doi.org/10.6084/m9.figshare.30152470.v1 (2025).

Acknowledgements

This work was supported by the National Institutes of Health/National Institute on Aging (NIH/NIA; grant numbers R01 AG038465 and R01 AG026158). ADNI: Data collection and sharing for this project were funded by the Alzheimer's Disease Neuroimaging Initiative (ADNI) (National Institutes of Health Grant U01 AG024904) and DOD ADNI (Department of Defense award number W81XWH-12-2-0012). ADNI is funded by the National Institute on Aging, the National Institute of Biomedical Imaging and Bioengineering, and through generous contributions from the following: AbbVie, Alzheimer's Association; Alzheimer's Drug Discovery Foundation; Araclon Biotech; BioClinica, Inc.; Biogen; Bristol-Myers Squibb Company; CereSpir, Inc.; Cogstate; Eisai Inc.; Elan Pharmaceuticals, Inc.; Eli Lilly and Company; EuroImmun; F. Hoffmann-La Roche Ltd and its affiliated company Genentech, Inc.; Fujirebio; GE Healthcare; IXICO Ltd.; Janssen Alzheimer Immunotherapy Research & Development, LLC.; Johnson & Johnson Pharmaceutical Research & Development LLC.; Lumosity; Lundbeck; Merck & Co., Inc.; Meso Scale Diagnostics, LLC.; NeuroRx Research; Neurotrack Technologies; Novartis Pharmaceuticals Corporation; Pfizer Inc.; Piramal Imaging; Servier; Takeda Pharmaceutical Company; and Transition Therapeutics. The Canadian Institutes of Health Research is providing funds to support ADNI clinical sites in Canada. Private sector contributions are facilitated by the Foundation for the National Institutes of Health (www.fnih.org). The grantee organization is the Northern California Institute for Research and Education, and the study is coordinated by the Alzheimer's Therapeutic Research Institute at the University of Southern California. ADNI data are disseminated by the Laboratory for Neuro Imaging at the University of Southern California.

Author contributions

Design of research: H.H., C.H., and Y.S.; methodology: H.H. and C.H.; formal analysis: H.H.; data collection: Y.S.; writing—original draft: H.H.; writing—review and editing: H.H., Q.R., Y.G., C.H. and Y.S.; funding and supervision: C.H. and Y.S.

Competing interests

The authors declare no competing interests.

Additional information

Supplementary information The online version contains supplementary material available at https://doi.org/10.1038/s43856-025-01170-5.

Correspondence and requests for materials should be addressed to Hengda He or Yaakov Stern.

Peer review information *Communications Medicine* thanks the anonymous reviewers for their contribution to the peer review of this work. [A peer review file is available].

for the Alzheimer's Disease Neuroimaging Initiative

Michael Weiner[6], Paul Aisen[7], Ronald Petersen[8], Clifford R. Jack Jr.[8], William Jagust[9], Susan Landau[9], Monica Rivera-Mindt[10], Ozioma Okonkwo[11], Leslie M. Shaw[12], Edward B. Lee[12], Arthur W. Toga[13], Laurel Beckett[14], Danielle Harvey[14], Robert C. Green[15], Andrew J. Saykin[16], Kwangsik Nho[16], Richard J. Perrin[17], Duygu Tosun[18], Pallavi Sachdev[19], Erin Drake[20], Tom Montine[21], Cat Conti[22], Rachel Nosheny[23], Diana Truran Sacrey[22], Juliet Fockler[18], Melanie J. Miller[22], Winnie Kwang[18], Chengshi Jin[18], Adam Diaz[22], Miriam Ashford[22], Derek Flenniken[22], Adrienne Kormos[22], Michael Rafii[7], Rema Raman[7], Gustavo Jimenez[7], Michael Donohue[7], Jennifer Salazar[7], Andrea Fidell[7], Virginia Boatwright[7], Justin Robison[7], Caileigh Zimmerman[7], Yuliana Cabrera[7], Sarah Walter[7], Taylor Clanton[7], Elizabeth Shaffer[7], Caitlin Webb[7], Lindsey Hergesheimer[7], Stephanie Smith[7], Sheila Ogwang[7], Olusegun Adegoke[7], Payam Mahboubi[7], Jeremy Pizzola[7], Cecily Jenkins[7], Naomi Saito[14], Kedir Adem Hussen[7], Hannatu Amaza[11], Mai Seng Thao[11], Shaniya Parkins[24], Omobolanle Ayo[24], Matt Glittenberg[11], Isabella Hoang[11], Kaori Kubo Germano[10], Joe Strong[11], Trinity Weisensel[11], Fabiola Magana[11], Lisa Thomas[11], Vanessa Guzman[24], Adeyinka Ajayi[24], Joseph Di Benedetto[24], Sandra Talavera[10], Joel Felmlee[8], Nick C. Fox[25], Paul Thompson[26], Charles DeCarli[14], Arvin Forghanian-Arani[8], Bret Borowski[8], Calvin Reyes[8], Caitie Hedberg[8], Chad Ward[8], Christopher Schwarz[8], Denise Reyes[8], Jeff Gunter[8], John Moore-Weiss[8], Kejal Kantarci[8], Leonard Matoush[8], Matthew Senjem[8], Prashanthi Vemuri[8], Robert Reid[8], Ian Malone[25], Sophia I. Thomopoulos[27], Talia M. Nir[27], Neda Jahanshad[27], Alexander Knaack[14], Evan Fletcher[14], Stephanie Rossi Chen[22], Mark Choe[22], Karen Crawford[27], Paul A. Yushkevich[12], Sandhitsu Das[12], Robert A. Koeppe[28], Gil Rabinovici[29], Victor Villemagne[30], Brian LoPresti[30], John Morris[17], Erin Franklin[17], Haley Bernhardt[17], Nigel J. Cairns[17], Lisa Taylor-Reinwald[17], Virginia M. Y. Lee[31], Magdalena Korecka[31], Magdalena Brylska[31], Yang Wan[31], J. Q. Trojanowski[31,49], Scott Neu[7], Tatiana M. Foroud[32], Taeho Jo[32], Shannon L. Risacher[32], Hannah Craft[32], Liana G. Apostolova[32], Kelly Nudelman[32], Kelley Faber[32], Zoë Potter[32], Kaci Lacy[32], Rima Kaddurah-Daouk[33], Li Shen[12], David Soleimani-Meigooni[18], Renaud La Joie[18], Konstantinos Chiotis[18], Maison Abu Raya[18], Agathe Vrillon[18], Charles Windon[18], Julien Lagarde[18], Zoe Lin[18], Aidyn Rose Hills[18], Jason Karlawish[12], Claire Erickson[12], Joshua Grill[34], Emily Largent[12], Kristin Harkins[12], Leon Thal[35], Zaven Kachaturian[36], Richard Frank[37], Peter J. Snyder[38,39], Neil Buckholtz[40], John K. Hsiao[40], Laurie Ryan[40], Susan Molchan[41], Maria Carrillo[42], William Potter[43], Lisa Barnes[44], Marie Bernard[45], Hector González[35], Carole Ho[46], Jonathan Jackson[47], Eliezer Masliah[45], Donna Masterman[48] & Nina Silverberg[45]

[6]University of California, San Francisco Northern California Institute for Research and Education, San Francisco, CA, USA. [7]University of Southern California, Los Angeles, CA, USA. [8]Mayo Clinic, Rochester, MN, USA. [9]University of California, Berkeley, CA, USA. [10]Fordham University, New York, NY, USA. [11]University of Wisconsin, Madison, WI, USA. [12]University of Pennsylvania, Philadelphia, PA, USA. [13]University of California, Los Angeles, CA, USA. [14]University of California, Davis, CA, USA. [15]Boston University, Boston, MA, USA. [16]Indiana University, Bloomington, IN, USA. [17]Washington University St. Louis, St. Louis, MO, USA. [18]University of California, San Francisco, San Francisco, CA, USA. [19]Eisai, Nutley, NJ, USA. [20]Harvard University, Cambridge, MA, USA. [21]University of Washington, Seattle, WA, USA. [22]Northern California Institute for Research and Education, San Francisco, CA, USA. [23]University of California, San Francisco, CA, USA. [24]Mt. Sinai, New York, NY, USA. [25]University College London, London, UK. [26]UCLA School of Medicine, Los Angeles, CA, USA. [27]University of Southern California School of Medicine, Los Angeles, CA, USA. [28]University of Michigan, Ann Arbor, MI, USA. [29]University of California San Francisco, San Francisco, CA, USA. [30]University of Pittsburgh, Pittsburgh, PA, USA. [31]UPenn School of Medicine, Philadelphia, PA, USA. [32]Indiana University School of Medicine, Bloomington, IN, USA. [33]Duke University/AD Metabolomics Consortium, Durham, NC, USA. [34]University of California, Irvine, CA, USA. [35]University of California, San Diego, CA, USA. [36]Khachaturian, Radebaugh & Associates (KRA), Inc., Potomac, MD, USA. [37]General Electric, Boston, MA, USA. [38]University of Connecticut, Storrs, CT, USA. [39]Alzheimer's Association's Ronald and Nancy Reagan's Research Institute, Chicago, IL, USA. [40]National Institute on Aging, Bethesda, MD, USA. [41]National Institute on Aging/National Institutes of Health, Bethesda, MD, USA. [42]Alzheimer's Association, Chicago, IL, USA. [43]National Institute of Mental Health, Bethesda, MD, USA. [44]Rush University, Chicago, IL, USA. [45]NIA, Bethesda, MD, USA. [46]Denali Therapeutics, South San Francisco, CA, USA. [47]Massachusetts General Hospital, Boston, MA, USA. [48]Biogen, Cambridge, MA, USA.